UNIVERSIDADE DE LISBOA

FACULDADE DE CIÊNCIAS

DEPARTAMENTO DE FÍSICA

Investigation of the Potential of Concomitant Radiation Therapy with Gold Nanoparticles for Pancreatic Cancer

Alexandra Vitória Figueiredo Martins

Mestrado em Engenharia Biomédica e Biofísica

Dissertação orientada por:
Brígida da Costa Ferreira, Ph.D., Prof.
Catarina Pinto Reis, Ph.D., Prof.

2022

Agradecimentos

Gostaria de expressar uma enorme gratidão para com a minha orientadora, Professora Brígida Ferreira, pelo apoio incondicional, pela paciência, pela disponibilidade, simpatia, e compreensão, e também por toda a atenção que pude receber da sua parte, nas muitas vezes que a procurei. Não posso também deixar de agradecer por todas as boleias que me ofereceu de e para a Fundação Champalimaud, e das conversas partilhadas durante as viagens.

Um muito obrigada à Dr.ª Sandra Vieira, Física-Médica na Fundação Champalimaud, pela enorme simpatia, generosidade e disponibilidade com que me recebeu sempre. Por me ter mostrado o funcionamento de um acelerador linear e por ter dado resposta a todas as minhas curiosidades. Um profundo agradecimento à Professora Manuela Gaspar, Investigadora do Grupo *Advanced Technologies for Drug Delivery* do iMed.ULisboa, pela simpatia com que me recebeu no Campus do Lumiar e pela imensa ajuda, apoio e disponibilidade que entregou a este projeto.

Um muito obrigada à minha orientadora, Professora Catarina Reis, pela simpatia, compreensão e disponibilidade durante o desenvolvimento deste trabalho. Não teria sido possível pôr este projeto em prática sem os protagonistas principais: as nanopartículas de ouro.

Não posso deixar de agradecer à Joana Lopes, doutoranda da FFUL, pela síntese das nanopartículas de ouro e por toda a ajuda que me deu no laboratório, e fora dele, sempre que precisei. Ao Pedro Farinha e à Jacinta Pinho, estudantes da FFUL, pela simpatia e boa disposição com que me receberam sempre nas instalações do Lumiar.

Um especial agradecimento ao Grupo de Ciências Radiofarmacêuticas do C2TN/IST pela enorme generosidade em cederem as suas nanopartículas de ouro para este projeto, em especial à Dra. Paula Campello e Dra. Alice D'Onofrio pela síntese das mesmas. Um obrigada à Professora Ana Viana, do Departamento de Química e Bioquímica da FCUL, pela imensa simpatia, pela ajuda durante o ensaio de Microscopia de Força Atómica, e por ter respondido com prontidão a todas as minhas curiosidades. E um obrigada ao Professor Rui Martins, do Departamento de Estatística e Investigação Operacional na FCUL, pela simpatia e ajuda prestada no que tocou à análise estatística dos resultados deste projeto.

Quero deixar os maiores agradecimentos aos meus pais e à minha irmã. Sem eles, o meu grande sonho de concluir um Mestrado não seria possível. Pelo apoio, a todos os níveis, pelo incentivo, pelas conversas e pelos conselhos. Às minhas amigas Luísa Freitas e Luísa Bia, quero agradecer por terem estado presentes quando mais precisei delas, e por todos os momentos bons que pudemos partilhar durante este último ano.

Abstract

Introduction: Pancreatic cancer is considered the seventh leading cause of cancer deaths worldwide. The lack of an effective treatment justifies the 5-year survival rates of less than 9%. Gold nanoparticles (AuNPs) may represent an opportunity to improve the quality of radiotherapy (RT) for pancreatic cancer patients. The present work consisted of an exploratory study aiming to evaluate the *in vitro* potential of concomitant RT with AuNPs in human pancreatic adenocarcinoma cells.

Materials and Methods: In this study, AuNPs with hyaluronic and oleic acids (HAOA-AuNPs) and AuNPs with bombesin (BBN-AuNPs) were used, and the cytotoxic effect of both formulations in BxPC-3 cells was assessed. Cells, with and without AuNPs at concentrations ranging from 50 to 200 μM, were irradiated with 6 MV X-rays at a 10 cm depth. Loss in cell viability induced by the combined treatment was evaluated 48 and 72 h after irradiation by MTT assay.

Results: Both HAOA-AuNPs and BBN-AuNPs alone induced cytotoxicity in a dose-dependent manner. At 72 h post-irradiation, a loss in cell viability of approximately 40% on average was obtained with RT plus 200 μM of HAOA-AuNPs when compared to the absence of any treatment (control) ($p < 0.0001$). Similar results were obtained for RT with BBN-AuNPs at 50 μM. In both situations, the effect of the combined treatment was seemed to be caused by an additive behaviour.

Conclusion: The post-irradiation incubation time is extremely relevant for the evaluation of cell viability by MTT assay. Here, the 72-h post-irradiation time proved to be the most appropriate to evaluate the effects of RT. As RT with AuNPs led to cell viability loss significantly different from the control, there appears to be a potential benefit from the combined treatment. Given the exploratory nature of this study, it is recommended to validate these results for other experimental conditions.

Keywords: Pancreatic cancer, Megavoltage radiation therapy, Gold nanoparticles, Cell viability, MTT assay.

Resumo

Introdução: O cancro pancreático é considerado a sétima causa de morte por cancro a nível mundial. O diagnóstico tardio da patologia e a inexistência de um tratamento eficaz justificam as taxas de sobrevivência a 5 anos inferiores a 9%. Os doentes com cancro do pâncreas localmente avançado e não ressecável, cerca de 30% a 40% dos doentes, podem ser considerados para quimioterapia ou quimiorradioterapia, resultando numa sobrevivência global média de 15 a 16 meses. A radioterapia (RT) visa melhorar o controlo local ou retardar a progressão da doença. Contudo, apesar das novas técnicas de RT, continua a ser problemática a administração de doses de prescrição de radiação mais elevadas sem causar toxicidade grave nos tecidos saudáveis mais próximos. Nanopartículas constituídas por um material de número atómico (Z) elevado, especialmente nanopartículas de ouro (AuNPs, Z = 79), têm sido cada vez mais estudadas no contexto da RT devido à possibilidade de aumentarem os efeitos da radiação quando introduzidas em células tumorais. Este aumento está relacionado com um acréscimo na libertação de fotoeletrões, eletrões de *Auger* e fotões de fluorescência, após eventos de ionização associados ao efeito fotoelétrico. Contudo, o tamanho, o revestimento, a forma, entre outras características das AuNPs, são altamente reveladores para um potencial aumento dos efeitos da RT. Para além disso, as células tumorais em causa e as características do feixe que irradia estas células podem também exercer um papel importante. Assim, encontram-se reportadas inúmeras formulações de AuNPs, bem como diferentes conclusões em relação ao sucesso do efeito combinado da RT concomitante com AuNPs. O presente trabalho consistiu num estudo exploratório com o intuito de avaliar o potencial *in vitro* das AuNPs durante o tratamento com Raios-X de 6 MV de células de adenocarcinoma pancreático humano BxPC-3, através de ensaios de viabilidade celular (ensaios MTT).

Materiais e Métodos: Neste estudo foram utilizadas AuNPs com ácidos hialurónico e oleico (HAOA-AuNPs) e AuNPs com bombesina (BBN-AuNPs). Recorreu-se às técnicas de Dispersão de Luz Dinâmica (*Dynamic Light Scattering – DLS*) e Microscopia de Força Atómica (*Atomic Force Microscopy – AFM)* para caracterizar as AuNPs em termos do seu tamanho e morfologia. A citoxicidade induzida por ambas as formulações de AuNPs nas células BxPC-3 foi avaliada recorrendo a incubação por 24 e 48 h com concentrações baseadas em ouro de 50, 200, e 400 μM. Foram realizados testes iniciais para avaliar o impacto que o transporte até ao local de irradiação teve nas células; bem como para selecionar a concentração celular e o tempo de incubação pós-irradiação ótimos a utilizar nos ensaios subsequentes. Foi construído um fantoma dedicado a este trabalho que maximizasse a reprodutibilidade do *setup* de irradiação e minimizasse o tempo de irradiação. Para estabelecimento das condições de irradiação, definiu-se como *standard* o seguinte *setup*: as células foram colocadas no isocentro a 10 cm de profundidade e irradiadas com um feixe fornecido por um acelerador linear Varian Edge de 6 MV com uma direção de irradiação posterior-anterior, um tamanho de campo de 20x20 cm^2, e taxa de dose de 600 MU/min. Nos ensaios que pretenderam avaliar o efeito de RT+AuNPs, as células BxPC-3 foram semeadas em placas de 96 poços a uma concentração de $8x10^4$ células/poço e após 24 h foram incubadas com 50, 200, e 400 μM de HAOA-AuNPs, e 50 e 200 μM de BBN-AuNPs por 4 h. Findo esse tempo, as placas de células foram irradiadas com doses que variaram de 2 a 10 Gy, dependendo do ensaio. Após irradiação, as células foram incubadas por 48 e 72 h até serem realizados os ensaios MTT. O impacto do espectro do feixe de radiação na RT com HAOA-AuNPs também foi testado através de duas condições: 1) variando os tamanhos de campo de 8x8 a 30x30 cm^2, e 2) para um feixe sem filtro aplanador (*free flattening filter – FFF)*. Por fim, foi realizada uma análise dosimétrica da distribuição de dose dos planos de RT utilizados durante as irradiações. Também foram testadas as distribuições de dose obtidas por dois planos baseados em

múltiplos segmentos, com o intuito de avaliar o seu potencial para irradiação de cada placa de células com vários valores de dose.

Resultados: Ambas as formulações de AuNPs apresentaram uma forma esférica. As HAOA-AuNPs possuem um diâmetro médio de aproximadamente 120 nm para as duas técnicas usadas e as BBN-AuNPs um diâmetro médio de 690 e 47 nm obtidos com *DLS* e *AFM*, respetivamente. O transporte revelou um impacto negativo na viabilidade celular e os ensaios de citoxicidade revelaram que ambas as formulações de AuNPs induziram citoxicidade dependente da concentração testada. Para além disso, as BBN-AuNPs induziram citoxicidade dependente do tempo de incubação. Os ensaios posteriores revelaram que, às 48 h após irradiação, houve perdas significativas na viabilidade celular de 20 a 30% com o tratamento combinado de 2 Gy com 50 ou 200 μM de HAOA-AuNPs em comparação com o controlo (ausência de qualquer tratamento). No entanto, este tempo de incubação pós-irradiação revelou-se demasiado curto para avaliar os efeitos da RT. Às 72 h pós-irradiação, uma perda significativa na viabilidade celular de aproximadamente 40% em média foi obtida com o tratamento combinado de RT com 200 μM de HAOA-AuNPs comparando com o controlo ($p < 0.0001$). Em relação às BBN-AuNPs, uma perda significativa na viabilidade celular de aproximadamente 45% em média foi obtida com o tratamento combinado de RT com 50 μM destas NPs ($p < 0.0001$). Para ambas as formulações, os efeitos do tratamento combinado 72 h após irradiação, parecem ter origem num comportamento aditivo dos efeitos da RT e das AuNPs. Não foi obtida uma relação entre o aumento do tamanho de campo e a perda de viabilidade celular para o tratamento de RT com AuNPs. Quando as células BxPC-3 foram irradiadas com um feixe *FFF*, às 72 h pós-irradiação obteve-se uma perda significativa na viabilidade celular de aproximadamente 40% em média para o tratamento combinado de RT com 200 μM de HAOA-AuNPs comparando com o controlo ($p < 0.0001$). Visto que foi obtida, em média, a mesma perda na viabilidade celular na situação com filtro aplanador (*standard setup*), a utilização do feixe *FFF* parece não ter originado um impacto diferente na viabilidade celular. Por fim, a análise dosimétrica confirmou que o plano *standard* de RT irradiou de forma homogénea todas as células incluídas nos vários poços da placa. Para além disso, os planos constituídos por múltiplos segmentos permitem uma irradiação homogénea com vários valores de dose das células em determinados grupos de poços cuidadosamente selecionados.

Conclusão: Com base nos resultados obtidos no presente estudo é de apontar que o tempo de incubação após irradiação é extremamente relevante para avaliação da viabilidade celular com ensaio MTT. Para este tipo de ensaios, um tempo de incubação de 72 h revelou ser o mais adequado para avaliar os efeitos da RT nas células. O tratamento combinado de RT quer com HAOA-AuNPs a 200 μM, quer com BBN-AuNPs a 50 μM, levou a perdas de viabilidade celular médias significativas quando comparado com o grupo de controlo que não recebeu qualquer tratamento. Este efeito pareceu ter tido origem num comportamento aditivo entre RT e as AuNPs. Assim, para ambas as formulações de AuNPs, parece haver um potencial benefício do tratamento combinado. Dado o carácter exploratório deste estudo, é recomendada a validação destes resultados, por exemplo, recorrendo a outro tipo de ensaios ou para outras condições experimentais. Seria também de grande valor realizar futuros testes para avaliar as possíveis razões químicas e/ou biológicas do efeito do tratamento combinado. Uma avaliação da distribuição celular das células BxPC-3 ao longo das fases do ciclo celular, por exemplo, seria bastante interessante. Assim como testar o potencial das AuNPs na irradiação de outras linhas celulares de células tumorais pancreáticas humanas.

Palavras-chave: Cancro pancreático, Radioterapia, Nanopartículas de ouro, Viabilidade celular, Ensaio MTT.

Table of Contents

List of Figures

List of Tables

List of Acronyms

3DCRT	Three-Dimensional Conformal Radiation Therapy
4DCT	Four-Dimensional Computed Tomography
AFM	Atomic Force Microscopy
AuNPs	Gold nanoparticles
BBN-AuNPs	Bombesin-coated gold nanoparticles
CRT	Chemoradiotherapy
CT	Computed Tomography
CUR	Curcumin
CV	Cell viability
DLS	Dynamic Light Scattering
DMSO	Dimethyl sulfoxide
DNA	Deoxyribonucleic acid
DSBs	Double-strand breaks
DSF	Disulfiram
DX%	Dose for which surviving fraction is X
EPR	Enhanced permeability and retention
FF	Flattening filter
FFF	Free-flattening filter
GEM	Gemcitabine
HA	Hyaluronic acid
HAOA-AuNPs	AuNPs coated with hyaluronic and oleic acids
IBR	Ibrutinib
IMRT	Intensity-Modulated Radiation Therapy
LAPC	Locally Advanced Pancreatic Cancer
LINAC	Linear Accelerator

MeOH	Methanol
MID	Mean Inactivation Doses
MRI	Magnetic Resonance Imaging
MTT	3-(4,5-dimethylthiazol-2-yl) 2,5-diphenyl tetrazolium bromide
NA	Not aplicable
NPs	Nanoparticles
NR	Not reported
OA	Oleic acid
PA	Posteroanterior
PBS	Phosphate buffered saline
PMMA	Polymethylmethacrylate
PdI	Polydispersity index
PEG	Poly(ethylene glycol)
ROS	Reactive oxygen species
ROSI	Rosiglitazone
RME	Receptor-mediated endocytosis
RT	Radiation Therapy
SSBs	Single-strand breaks
SS-BBN	Thioctic acid terminated bombesin peptide
SBRT	Stereotactic Body Radiation Therapy
SF	Surviving fraction
SFX	Surviving fraction of cells irradiated with X Gy
TDOTA	2-[4,7-bis(carboxymethyl)-10-[2-(3-sulfanylpropanoylamino) ethyl]- 1,4,7,10-tetrazacyclododec-1-yl] acetic acid
Z	Atomic number

1. Introduction

1.1. Pancreatic cancer

The pancreas is a roughly hammer-shaped organ measuring 14-20 cm in average for an adult and is anatomically divided into three main sections: head, body, and tail (Figure 1.1), being the uncinate process an extension of pancreatic head with varying prominence. This gland is deeply located in the retroperitoneum in direct contact with organs and structures such as the vertebral column, liver, stomach, duodenum, kidney, and aorta. It has exocrine and endocrine tissues in its constitution, which are related to the digestive and hormonal functions, respectively. Exocrine pancreas is responsible for the production of enzymes such as lipases and peptidases, while hormone production includes insulin and glucagon [1].

According to World Health Organization 2020 estimates, 495 773 new pancreatic cancer cases were diagnosed, and 466 003 patients died from this disease [2]. In that year, it was considered the seventh leading cause of cancer-related deaths worldwide [2]. Exocrine pancreatic cancer constitutes most of the pancreatic malignancy (up to 95%) and, of those, 90% are adenocarcinomas originating from ductal epithelial cells [3,4].

Pancreatic cancer incidence is rising in the developed world, and risk factors such as alcohol abuse, dietary factors, tobacco smoking, obesity and family history were identified [5,6]. Because of the late diagnosis of this pathology and the ineffectiveness of available treatments, especially in advanced stages, the prognosis is still extremely poor, with five-year survival rates below 9% [5,6]. Therefore, there is a large need to investigate new treatment approaches that meet the existing challenges aiming to improve overall survival and patients' quality of life.

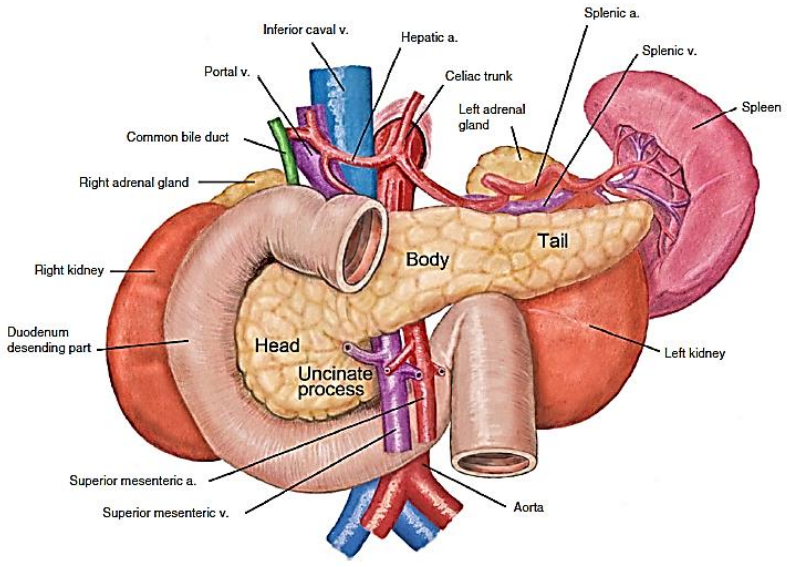

Figure 1.1 – Localization of the pancreas and its relationship with the surrounding organs and blood vessels. Figure extracted from Campbell *et al.* (2013) [1].

Rapid diagnosis is crucial for the selection of patients who are candidates for surgical resection (stage I-II) [4,7]. Resectability criteria are based on tumour involvement along nearby arteries and veins which can be assessed with abdominal Computed Tomography (CT) or Magnetic Resonance Image (MRI) [7]. Despite being the only strategy that contributes to long-term overall survival in this disease (about 20 months), after a surgical resection, patients still have a high rate of local recurrence and a high-risk of develop distant metastasis [7]. Consequently, patients with resectable disease (about 20% of pancreatic cancer patients) also receive adjuvant chemotherapy [7,8]. The recommended chemotherapy regime is modified FOLFIRINOX (fluorouracil, oxaliplatin, irinotecan and leucovorin) for patients suitable for this protocol or gemcitabine/capecitabine or gemcitabine alone for patients with poor functional status [9].

Patients with locally advanced unresectable pancreatic cancer, about 30% to 40% of patients, present with a tumour involving the celiac trunk or the superior mesenteric artery [4]. These patients can be considered for chemotherapy or chemoradiotherapy (CRT), resulting in a median overall survival of 15 to 16 months [7]. If down-staging of the tumour occurs after primary treatment, a resection may then be performed [8]. However, only 20% of patients are likely to have sufficient tumour response and become eligible for surgery [9].

Approximately 40% to 50% of patients present with metastatic disease and these are generally best managed with systemic chemotherapy. The peritoneum, liver and lungs are the most frequent metastatic sites [4]. Short courses of radiotherapy (RT) for pain relief may be recommended. Median survival is of less than one year even when these patients are treated with modern chemotherapy regimens [7]. Multiagent chemotherapy regimens for patients with locally advanced and metastatic disease include FOLFIRINOX or gemcitabine and albumin-bound paclitaxel (gemcitabine/nab-paclitaxel). These treatment regimens represent a survival benefit of 2 to 6 months when compared to single-agent gemcitabine [9]. However, none of them is totally effective in treating locally advanced and metastatic pancreatic cancer.

The role of radiation therapy in pancreatic cancer is still unclear, and CRT for locally advanced pancreatic cancer (LAPC) is controversial. While some studies have shown clinical advantages to the addition of RT to the treatment, others report no significant improvements [10]. Nonetheless, these outcomes highly depend on patient selection criteria and the RT technology used, for instance, the consideration of the motion of the pancreas during irradiation. All these factors may explain why RT treatment was considered ineffective in some cases [10]. In addition, pancreatic cancer is a deep-seated tumour and its involvement with radiosensitive organs severely limits the prescribed radiation dose. This constitutes a relevant constraint to the success of the treatment. Still, RT aims to improve local control, delay disease progression, and ameliorate locally obstructive symptoms [11], and current guidelines support CRT as an option in LAPC when chemotherapy alone is not effective [9].

For the accurate delivery of individualized RT treatment, a CT is acquired with the patient in the supine position with arms above head [7]. The use of contrast is helpful to define the target and to detect both vascular landmarks and radiosensitive structures, such as the duodenum, stomach, aorta, and kidneys [4,7]. Due to respiratory motion, pancreas and nearby structures move, so 4D Computed Tomography is being increasingly used [7]. For conventional RT techniques, prescription radiation dose varies between 45 – 54 Gy delivered in 25 – 30 fractions, depending on the stage of the tumour and its proximity to critical tissues [10,11]. For CRT, chemotherapy acts as a radiation sensitizer (small doses are delivered concurrently to the RT treatment). Due to long period of treatment of this

fractionation scheme, there is a delay in the delivery of full-dose chemotherapy when this regimen is recommended [10].

3D-Conformal Radiation Therapy (3D-CRT) is the most common RT technique. In this case, using 3D anatomical data acquired from CT and/or MRI, the beam cross section is designed to be conformal to the target volume [4]. Common side-effects with this technique are nausea and vomiting, diarrhoea, and gastrointestinal bleeding/duodenal ulcer [12]. In turn, Intensity-Modulated Radiation Therapy (IMRT) provides a highly conformal dose distribution to the target volume through the use of multiple beams with non-uniform intensities, using either static or dynamic segments [4].

Stereotactic Body Radiation Therapy (SBRT) is the most recent technique, and it is increasingly being used for pancreatic cancer. In contrast to the two previous techniques, SBRT is based on the use of ablative doses of radiation (ranging 6 – 33 Gy) delivered with a small number of fractions (1 – 5) [10]. Due to the necessity of high precision for this technique, optimal patient immobilization, motion management, and accurate targeting is required [7]. SBRT has shown to be promising for LAPC because it presents with shorter treatment courses, better local control, minimal acute side effects, and earlier start of full-dose chemotherapy [7,11].

However, despite the improvement in the quality of RT techniques, no significant improvements in patients' overall survival were obtained. A systematic review from the literature reported mean overall survival for 3D-CRT, IMRT, and SBRT to be 11.7, 13.8, and 13.1 months, respectively [13]. Nevertheless, this review has shown statistically significant improvements in local tumour response achieved with SBRT (average response rate of 27.3, 37.2, and 57.2%, for 3D-CRT, IMRT, and SBRT, respectively) [13].

1.2. Motivation

Despite the most recent advances in CRT, including alternative cytotoxic agents (e.g., FOLFIRINOX) and new RT techniques (e.g., SBRT), pancreatic cancer is still one of the deadliest cancers [5]. In part due to the lack of appropriate diagnosis and consequently late detection of this pathology, but also due to the inability to deliver higher doses of RT locally without causing severe toxicity to nearby healthy tissues [6]. The ability to successfully improve local tumour response may lead to an extension of the overall survival. As pancreatic tumour response is dose-dependent [10], improving RT by allowing a local dose escalation while maintaining or reducing the dose in nearby organs at risk, could potentially result in a better treatment outcome.

Nanoparticles (NPs) with high atomic number (Z), such as gadolinium (Z=64), hafnium (Z=72), platinum (Z=78), and gold (Au) (Z=79) have been increasingly studied in the context of RT as radiation sensitizers due to their capacity to enhance radiation effects locally when introduced into tumour cells [14–17]. The basic principle is related to the high potential of these high-Z NPs to absorb low-energy X-rays, consequently leading to atomic excitation, and an increase of electrons release into the medium compared to soft tissue. Enhancement of electrons release (ionisation events) translates into a local increase of energy deposition, which causes a larger damage to tumour cells compared to RT alone. This will be explained in detail in section 1.4.

Gold NPs (AuNPs) are the most studied NPs for RT due to their high-Z, good biocompatibility, and low-cost production process [14–17]. Moreover, they have also been studied for other biomedical applications, such as imaging (as a CT contrast agent) and drug-delivery (also interesting in the context of CRT) (Figure 1.2). AuNPs are colloidal or clustered particles with diameters generally ranging from 1-150 nm that consist of a gold core with a surface coating. Owing to their synthetic versatility, it is possible to obtain a design with different sizes, shapes, and surface coatings. The manipulation of the size and shape allows the production of AuNPs with specific chemical, electrical, and optical properties. Coating offers the possibility to control particle solubility, stability, and interaction with biological environment [15]. These are factors of great importance, since they dictate the fate of the NPs and, consequently, their accumulation in the tumour.

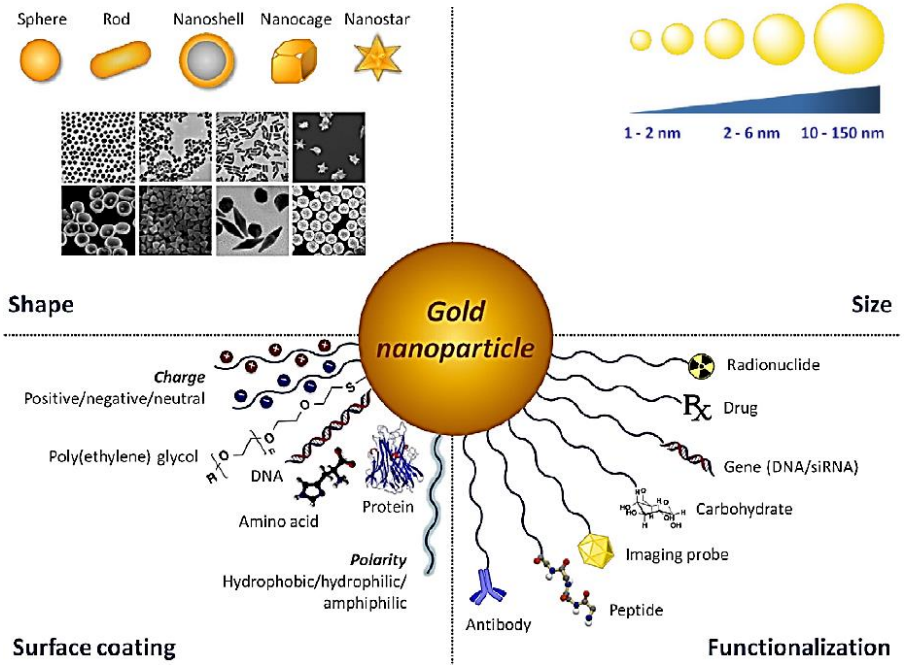

Figure 1.2 – AuNPs present with synthetic versatility which enables their design with different sizes, shapes, surface coating, and functionalization, making possible a production adapted to the needs. Figure adapted from Her *et al.* (2015) [15].

This work reports an exploratory study for assessing the *in vitro* potential of concomitant RT with AuNPs (i.e., RT applied simultaneously with AuNPs) in BxPC-3 human pancreatic adenocarcinoma cells with MV X-rays. Initially, a protocol for irradiation and cell culture was developed. To accomplish this goal, a phantom to be used during cells irradiation was designed and irradiation setup was defined. Both the number of BxPC-3 cells to be seeded per well of a 96-well plate and the incubation time post-irradiation were studied.

AuNPs cytotoxicity on BxPC-3 cells was assessed after incubation with several gold-based concentrations. For this, AuNPs with a coating of hyaluronic acid (HA) and oleic acid (OA) – HAOA-AuNPs – and AuNPs coated with bombesin – BBN-AuNPs – were used. The impact of both AuNPs formulations during RT was then assessed by cell viability assays. Also, the influence of beam spectra on the potential of HAOA-AuNPs was studied by varying field size and removing the flattening filter from the beam path. Finally, a dosimetric analysis was carried out to assess the homogeneity of the dose distribution of the RT plans used.

1.3. Cellular internalization of AuNPs

When developing AuNPs, a balanced design between biodistribution and radiation sensitizing properties need to be addressed; and the optimal concentration needed to maximize radiosensitization while minimizing toxicity to the healthy tissues must be determined [17]. There are numerous AuNPs formulations reported for cancer RT [14–17]. However, outcomes for AuNPs radiosensitizer ability vary among the different studies. Different tumour microenvironments interfere differently with NPs penetration into the tumour interstitium and, consequently, their uptake by tumour cells. Thus, outcomes between different types of cancer should be compared with caution. To maximize the efficacy of radiosensitization by AuNPs, not only nanoparticle parameters are key, but also the conditions of the RT treatment play a very important role. These include the beam modality and energy, irradiation depth, etc [14,15,18–20].

In vitro cellular internalization of AuNPs, possible due to receptor-mediated endocytosis (RME), is necessary to achieve radiosensitization [15]. RME is an energy-dependent process where internalization of NPs occurs after cell surface receptors bind to specific molecules on the surface coating of NPs, the so-called ligands (Figure 1.3). After binding, endosomal vesicles containing the NPs will later fuse with lysosomes leading to their excretion [16].

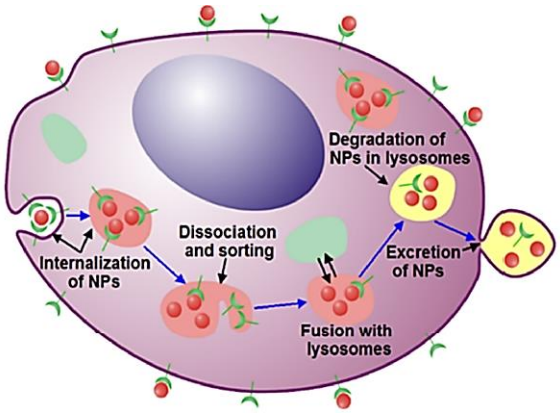

Figure 1.3 - Process of cellular internalization and excretion of AuNPs. Figure extracted from Bromma *et al.* (2020) [16].

Size and shape are decisive factors for AuNPs internalization into cell via RME. The size dependence is associated with the need to recruit receptors from farther away when endocytosis of larger particles is being performed [17]. Shape dependence is related to AuNPs surface area and local curvature, both interfering in the interaction of their ligands with the cell membrane receptors [17]. Spherical AuNPs are the most common in gold-based nanotherapeutics as they are simple to produce, and alteration of size and surface chemistry is easily achieved [16].

Entry into the cell nucleus translates into further increased damage during RT due to the proximity of the AuNPs to the Desoxyribonucleic acid (DNA) (explained in more detail in section 1.4) and, consequently, the possibility of DNA damage being more fatal to the cell. However, entry into the nucleus is not simple, and conjugate AuNPs with specific peptides, such as the nuclear localization sequence, may be a good strategy [17]. Also, it was reported that NPs must be smaller than about 30 nm to allow importation through the nuclear pore complex [15].

In vivo cellular internalization is much more complex. Both AuNPs toxicity and circulatory half-life become extremely relevant, as they have direct impact on patient wellbeing and efficacy of radiosensitization, respectively. Also, depending on the mode of administration, AuNPs face many challenges until reaching the tumour site. After intravenous administration, AuNPs must pass through the blood circulation, accumulate in the tumour, penetrate it, be internalized by tumour cells, and avoid clearance for as long as necessary to obtain effective radiosensitization during RT [15].

Once in the bloodstream, AuNPs will have to avoid binding with serum proteins and ions to avert destabilisation of their surface and consequent aggregation [15]. If aggregation occurs, AuNPs will be removed from the circulatory system by macrophages [16]. It was reported that functionalization with poly(ethylene glycol) (PEG) – process called PEGylation – increases blood circulation time of NPs, since it prevents protein adsorption and clearance by macrophages [16].

NPs have a preferred accumulation in the tumour via a phenomenon known as enhanced permeability and retention (EPR) effect [17]. This is explained by their small size compared to the typical cut-off size of tumour vasculature pores ($\leq$ 400 nm) which leads to a "passive targeting" of NPs to the tumour [17]. However, EPR effect is still quite controversial. Particularly, in advanced human tumours (such as LAPC), where obstructed tumour blood vessels and supressed blood flow determine a heterogeneity of the EPR effect. This leads to both inefficient accumulation and intratumoural distribution of NPs [21].

Instead, "active targeting" may be more efficient to obtain an intratumoural accumulation of AuNPs. In this strategy, AuNPs surface are functionalized with peptides or antibodies that will later bind to cell surface proteins (receptors) preferentially overexpressed by cancer cells – tumour-targeted AuNPs. This translates into 1) getting a higher concentration of AuNPs within the tumour compared to healthy tissues; and 2) a reduced quantity of gold needed for radiosensitization [17]. Hyaluronic acid (HA) is a natural mucopolysaccharide, highly biocompatible, that specially targets CD44, a receptor expressed by a wide range of tumours [22,23], including pancreatic adenocarcinomas [24,25]. Thus, conjugate AuNPs with HA may lead to a preferred accumulation of NPs into pancreatic tumour cells via RME, which in turn would translate into further harm to these cells during RT.

Finally, clearance of AuNPs is mainly done via kidneys and via liver. AuNPs of smaller size are excreted by renal clearance (within hours to days after administration) [26], while AuNPs larger than the renal filtration cut-off accumulate in the reticuloendothelial system – composed by liver, spleen, and lymph nodes – after opsonization [15,17]. This accumulation may last for days before excretion occurs, or even months in the case of the liver [17]. This brings up critical issues related to patient health, including histological alterations, and secretion of inflammatory cytokines resulting in apoptosis of liver cells [17]. Thus, it is of immense importance to optimize NPs features such as size and surface coating to avoid a pathological accumulation along reticuloendothelial system organs.

1.4. Mechanisms of AuNPs radiosensitization

The three main types of interaction of photons with matter are: photoelectric effect, Compton effect, and pair production. [4]. In the photoelectric effect, the incident photon ionizes an atom by removing an electron (named as photoelectron) typically from an inner orbital. It is dominant for low-energy X-rays (typically up to ≈ 500 keV) and in high-Z materials [14]. Depending on the energy of the incident photon, the photoelectron can travel up to a distance of one to several cells. Atom de-excitation occurs via fluorescent photon emission or Auger electron emission. Typical Auger electrons have energies lower than 100 eV having ranges of less than 10 nm in tissue [14]. Consequently, these short-range low-energy electrons offer a very precise and local dose deposition [27]. Thus, AuNPs size and coating strongly impact on how many of these Auger electrons can effectively escape from the NP [14].

The probability of the radiation interacting with the material is positively correlated with the fourth power of atomic number (Z^4) of material, and the third power of wavelength (λ^3) of radiation [4] – Figure 1.4 (based on [28]). For energies < 500 keV, the probability of photoelectric effect is significantly higher in gold than in tissue or water (Z=7.5) [29] leading to a greater release of photoelectrons, fluorescent photons, and Auger electrons in the vicinity of AuNPs. Auger electrons are especially responsible for depositing energy in the vicinity of AuNPs, while photoelectrons will deposit their energy further away [14]. Thus, when tissues are irradiated in the presence of AuNPs, there will be an increase in dose deposition to tumour cells when compared to when AuNPs are absent. In addition, since fluorescent photons can travel large distances, they are able to ionize other gold atoms and proceed with this cascade of electrons release [14].

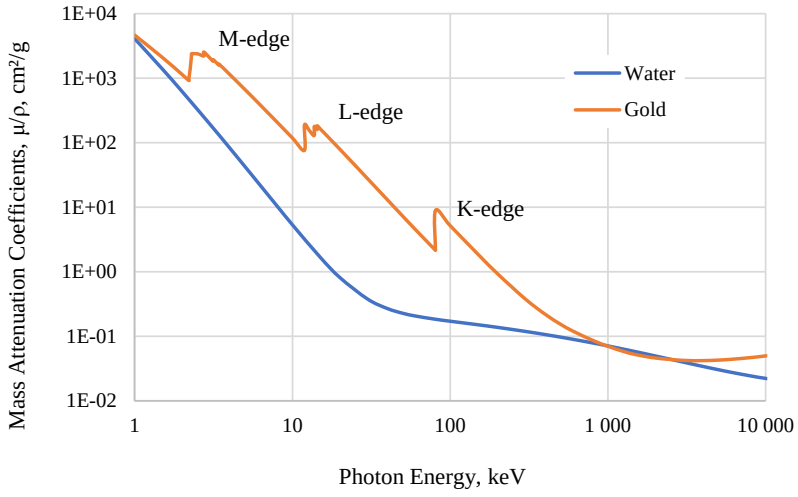

Figure 1.4 - Total mass attenuation coefficient, μ/ρ, for different photon energies for water and gold. Photoelectric effect is dominant for X-rays energies < 500 keV and for high atomic number (Z) of material. For the range of energies used in RT, Compton effect is predominant. This effect does not depend on Z, thus, changes on beam attenuation for water and gold are not distinguishable (the lines merge). M-, L-, and K-edges represent the subatomic shells of the atom. Graphic constructed based on the μ/ρ values presented in [28].

Compton effect is the predominant effect for high-energy X-rays (> 500 keV), being the main mechanism of absorption of ionizing radiation with clinical photons beams [14] (Figure 1.5). This effect consists of a photon collision with a free electron from an outer orbital that is ejected from the atom. The photon is then scattered with a lower energy. Compton effect does not depend on Z; however, it does depend on the electron density of the material [4]. Consequently, because of the availability of multiple electrons in the outer shells of gold atoms [14], the effective probability of a Compton scatter interaction in the presence of AuNPs may be higher compared to soft tissues. This could lead to an increase in collisions and a greater release of electrons and attenuated photons. Additionally, as in each collision the photon loses energy, with increasing depth there is an increase in the probability of occurring photoelectric effect [14]. Finally, for clinical MV X-rays beams, pair production also occurs. However, this phenomenon is less important than Compton effect at clinically relevant energies (< 10 MeV) [14].

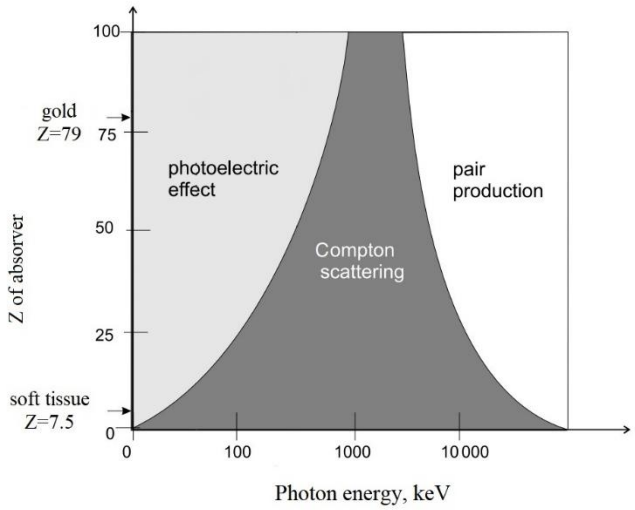

Figure 1.5 - Predominance of photoelectric effect, Compton effect, and pair production for Z of absorber against photon energy (keV). Compton effect is the main mechanism for the absorption of ionizing radiation in RT for both gold and soft tissue. Figure adapted from Powsner *et al.* (2006) [29].

In RT, the radiation beam is composed by a photon beam spectrum up to a maximal energy of 6 MeV, in the case of this work. Variations in beam spectra due to increased depth or variations in field size might contribute to the potential of AuNPs. For instance, larger field sizes generate greater scatter radiation leading to an increase in the number of low energy photons in the beam spectrum [19,20]. Also, other studies have reported that the beam produced by LINAC with free-flattening filter have a higher proportion of low-energy photons in the primary path than a beam produced with flattening filter. In the presence of AuNPs, these low-energy photons contribute to an increase in photoelectric interaction, which may lead to an enhancement of RT+AuNPs effects [18–20].

These physical processes, contributing to radiosensitization, occur in the first picoseconds of exposure to ionizing radiation [30]. In the next milliseconds, the chemical phase takes place. Radiation can cause damage to the DNA molecule through its ionisation (direct damage) or through the formation of free radicals by ionisation of water molecules (indirect damage) [4]. Through the fixation of these free radicals to soluble oxygen present in tissues, more stable and toxic radicals are formed – reactive oxygen species (ROS) [4]. ROS can potentially cause cellular damage directly by ionising the

DNA molecule, which constitutes the main mechanism of radiation-induced cell death [15,31]. DNA damage predominantly consists of single strand breaks (SSBs) – breaks in a single DNA strand – which are more probable to be repaired by the cell than double strand breaks (DSBs) – breaks in both DNA strands [4].

When AuNPs are associated with RT, the increased release of photoelectrons, Auger electrons, and fluorescent photons due to photoelectric effect, as well as release of recoil electrons and scatter photons from Compton effect, establishes a highly reactive environment. This leads to increased radiolysis of water molecules and, consequently, to an enhanced production of ROS in the vicinity of the AuNPs. Additionally, the surface of AuNPs is electronically active and it is capable of catalysing chemical reactions through interactions with molecular oxygen [15,16]. This interaction facilitates surface-mediated transfer of electrons to molecular oxygen, which leads to ROS production. In combination with RT, the catalytic properties of AuNPs have shown to be further enhanced by interacting with the highly reactive environment [15,16]. Thus, AuNPs constitute a chemical sensitisation of DNA molecules to RT – there is an increased likelihood of DNA ionisation by secondary electrons and ROS [14–16].

Finally, in the biological phase – which lasts seconds to years (in case of carcinogenesis caused by RT to healthy tissues) – irradiated cells activate a DNA-damage response that consists of sensors and effectors [30]. The initial cellular response to DSBs is characterized by the recruitment of different proteins to the sites of DNA damage, process commonly referred to as ionizing radiation induced 'foci'. This process starts after the phosphorylation of histone H2AX (sensor of damage), γH2AX, which can be detected using microscopy. After phosphorylation of recruited proteins, DNA-damage response effectors – cell-cycle checkpoints, DNA repair, and cell death (if DNA cannot be repaired) – are activated [4,30].

The levels of intracellular ROS induced by AuNPs may also have biological consequences due to oxidative stress. This cause impairment of mitochondria and oxidizing of cellular components including the DNA, lipids composing the cell membrane and proteins, triggering cell death via apoptosis and/or necrosis [15,16,26]. Oxidative stress is considered one of the most salient features of AuNPs cytotoxicity [15,32], and has been evidenced to depend not only on AuNPs shape, coating, size or applied concentration, but also on the cell line studied [26,32,33]. Generally, the smaller the size of the AuNP, the higher its cytotoxic effect. This is due to the high surface area relative to their volume increasing the chances of interact with biomolecules [26]. Since an increase in ROS is expected to occur in combination with RT, the chances of the cell dying by apoptosis and/or necrosis due to oxidative stress are also increased. Thus, the intrinsic cytotoxicity of AuNPs may also constitute a form of radiosensitization to tumour cells.

Lastly, another possible biological pathway of radiosensitization identified for AuNPs is the cycle arrest in the G2/M phase due to changes in the expression levels of cyclin kinases (which are involved in the regulation of the cell cycle) [15,32]. Cells in late G2 and mitosis (M) phases are highly radiosensitive, while cells in late S phase are more radioresistant [4,15]. Thus, depending on the cell line and AuNPs features such as size and coating, AuNPs could "block" cells within the G2/M phase and lead to enhanced cell sensitivity to X-rays during RT, causing greater cell death [15,16].

The three described mechanisms, i.e., the physical, chemical and the biological, all contribute to tumour cell radiosensitization by AuNPs [14–16]. However, the intrinsic cytotoxicity of AuNPs has also been detected in healthy cells [34,35]. This constitutes a major problem, as toxicity in healthy

cells may lead to cell death. Thus, during a study, cell viability assays evaluating the cytotoxicity of AuNPs in tumour and non-tumour cell lines should ideally be performed. Furthermore, in a way to avoid off-target accumulation *in vivo*, the physicochemical characteristics of AuNPs should also be carefully studied.

1.5. State of the art

The possibility of applying AuNPs to RT for cancer treatment has been widely studied over the last years through simulation studies, *in vitro* and *in vivo* studies, and some pre-clinical studies [14–17,31]. In the present chapter, simulation studies will be superficially covered and, subsequently, a more detailed analysis of the most recent *in vitro* studies addressing the use of AuNPs in the irradiation of tumour cells with kV and MV X-rays will be performed. Studies that have evaluated the potential of AuNPs with RT through cell survival assays and cell viability assays will be addressed.

Monte Carlo simulations can be used to model the physical and physicochemical processes of radiation interactions with matter, including biological targets. This provides valuable insights into estimating AuNP-induced dose enhancement and ionisations for a range of parameters, such as AuNP size, shape, radiation source and energy, etc [14].

Several studies have shown that the dose enhancement depends on the location and size of the AuNP, among other important physical factors [14]. Most studies are consistent in arguing that to maximize tumour cell kill, AuNPs need to be in close proximity to the nucleus DNA [14]. However, McNamara *et al.* has shown, using a realistic compartmentalised cell model, that the dose enhancement caused by 1% of gold in cytosol was greater in the mitochondria than in the nucleus [14]. This was due to the larger surface area to volume ratio of the mitochondria indicating that mitochondria and mitochondria DNA are also viable radiation targets.

Studies assessing dose enhancement by AuNPs using 80–120 kV beams obtained a dose enhancement factor near 2 [14]. However, based solely on physical dose enhancement, radiosensitization with AuNPs is expected to be insignificant at clinical MV X-rays due to the minimal contribution of photoelectric effect [15]. In fact, simulation studies assessing MV beams showed negligible dose enhancement by AuNPs [14]. For instance, Lechtman *et al.* concluded that AuNP radiosensitization using a 6 MV source is not clinically feasible because of the unacceptably high concentration of AuNP required – approximately 1600 mg Au/g of tumour is needed to double the conventional fraction dose of 2 Gy [14]. Other theoretical predictions by Monte Carlo simulations calculated dose enhancement factors of 1.007–1.014 for 6 MV compared to 2.114 for 140 kV assuming 7 mg Au/g of tumour [15].

Interestingly, the first experimental studies using MV X-rays beams with AuNPs showed an enhancement of RT effects that were significantly higher than those estimated by Monte Carlo simulations [15]. Chithrani *et al*. observed a dose enhancement of 1.17 for 6 MV, and Jain *et al.* achieved gains of 1.29 and 1.16 for 6 and 15 MV, respectively. The discrepancies between theoretical predictions and experimental data opened the door to the possibility of chemical and/or biological enhancement in addition to the physical mode of action [15]. Nevertheless, biological outcomes cannot yet be directly simulated by Monte Carlo simulations without the validation of accurate

biological models. Thus, *in vitro* studies are needed to characterise cellular-scale impact of AuNPs including cell toxicity, uptake dynamics, radiation-induced cell survival, etc.

The *in vitro* radiosensitizer effect of AuNPs has been increasingly studied for the treatment of various human tumour cell lines including breast, lung, colon, cervix, and brain [36–41]. Table 1.1 compiles the most recent studies, published since 2015, on irradiation of these human tumour cell lines with kV X-rays assessed through clonogenic assays. Most authors estimated the gain factor conferred by AuNPs to RT using different models making comparisons between studies difficult. The lack of a standard methodology to evaluate the radiobiological effectiveness of AuNPs may constitute an obstacle for the transition into clinical practice [42].

Chen *et al*. obtained a gain of 1.37 for the U87 glioblastoma cell line irradiated with 160 kV and 28 nm AuNPs. No changes in cell viability after the incubation with different AuNPs concentrations for 24 h were obtained. It was verified that AuNPs increased the density of the γH2AX foci - which is correlated to the density of DSBs – at 0.5 and 2 h post-irradiation. Also, a significant increased ratio of cell apoptosis was found 48 h after irradiation with AuNPs, meaning that there was no repair of DNA damage, which led to cell death [36].

Both Hau and Liu *et al.* used 50 kV to irradiate a colon (LOVO) and cervix (HeLa) cancer cell lines, respectively. Liu *et al.* obtained gains ranging from 1.14 to 2.88 after testing three different concentrations of AuNPs with ~15 nm. Cytotoxicity tests evaluated cell viability after a 24 and 72 h incubation with various concentrations of AuNPs. After 24 h, cell viability was even higher than that of the control; however, after 72 h, cell viability decreased. In addition, it was assessed the effect of AuNPs on the cell cycle and it was concluded that NPs did not lead to an accumulation of cells in the G2/M phase [37]. Hau *et al.* showed a gain of 18.3% after irradiation with 10 nm AuNPs. No effect of AuNPs alone was shown on cell viability after incubation with different concentrations for 24 – 96 h [38].

Özçelik *et al.* investigated the benefits of AuNPs to treat the A549 lung cancer cell line with a photon beam of 225 kV. A gain ranging from 1.20 to 1.55 was obtained after the administration of different concentrations of 40 nm AuNPs specially targeting the nucleus [40]. Soleymanifard *et al.* irradiated another lung cancer cell line (QU-DB) with 100 kV after the administration of AuNPs with 16 nm, and a gain of 64.4% was obtained. Under the same experimental conditions, the MCF-7 breast tumour cell line was also irradiated, which conducted to a similar gain. Cytotoxicity tests using different concentrations were performed, and AuNPs alone did not induce remarkable toxicity on both cell lines after 2 h incubation. However, no further tests were performed to analyse the possible biological causes of the radiosensitization effect [39].

Finally, Tudda *et al.* irradiated the MDA-MB-231 breast tumour cell line with 190 kV after the administration of 15 nm AuNPs. A negligible gain of 1.08 was obtained for the lowest concentration of AuNPs, which raised to 1.20 by increasing the concentration to 200 μg/mL. Interestingly, in this study, gain was also estimated using a second expression which resulted in a value of the gain of 1.15 and 1.33, respectively. No cytotoxic effect of AuNPs alone was observed on cell viability after 24 h incubation with different concentrations [41]. No further studies were performed to analyse the possible biological cause of the radiosensitization effect obtained.

Table 1.1 - Summary of *in vitro* studies assessing AuNPs radiosensitization with 50 to 225 kV X-rays through clonogenic assay.

Author	Cell Line	X-rays (kV)	NP Size (nm)	Concentration(s) (μg/mL)	Gain factor	Model used
Tudda ***et al***. (2022)	MDA-MB-231 (Breast)	190	15	100 200	(1): 1.08 1.20 (2): 1.15 1.33	(1) $\frac{\text{MID (RT)}}{\text{MID (RT+NPs)}}$ (2) $\frac{D_{40\%}(\text{RT})}{D_{40\%}(\text{RT+NPs})}$
Özçelik ***et al***. (2020)	A549 (Lung)	225	40	1 3 10	1.20 1.38 1.55	$\frac{D_{10\%}(\text{RT})}{D_{10\%}(\text{RT+NPs})}$
Soleymanifard ***et al***. (2017)	MCF-7 (Breast) QU-DB (Lung)	100	16	19.7×10^3	64.1% 64.4%	$\frac{SF2(RT)-SF2(RT+NPs)}{SF2(RT)}$ (%)
Hau ***et al***. (2016)	LOVO (Colon)	50	10	50	18.3%	NR
Liu ***et al***. (2015)	HeLa (Cervix)	50	15	1.5 7.5 15	1.14 2.88 1.86	$\frac{D_{50\%}(\text{RT})}{D_{50\%}(\text{RT+NPs})}$
Chen ***et al***. (2015)	U87 (Brain)	160	28	36	1.37	$\frac{SF2(RT)}{SF2(RT+NPs)}$

Abbreviations: MID = Mean Inactivation Doses, i.e., area under the survival curves; DX% = dose for which surviving fraction is X%; SFX = surviving fraction of cells irradiated with X Gy; NPs = nanoparticles; RT = radiotherapy.

Table 1.1 reports only some of the factors that may impact in treatment success. However, many other features may have a significant impact on the value of the gain factor – the coating of AuNPs, the time they were in contact with cells before irradiation, the incubation time after irradiation until the assays were performed, among others. In addition, few studies fully report the conditions under which irradiation was performed, for example, use of flattening filter, depth of irradiation, or field size. However, these parameters may also influence the value of the gain obtained when adding AuNPs to RT [18–20]. In addition, all authors used different models to calculate the value of the gain making it very difficult to assess which set of conditions exponentiates the effects of AuNPs.

Concomitant AuNPs-RT with kV beams have shown some promising results. However, low-energy photons are not suitable for the treatment of deep-seated tumours, pancreatic cancer included. The greater penetration power of MV photon beams, increasing with energy, make this beam quality preferable for clinical RT of most pathologies [4] (Figure 1.6).

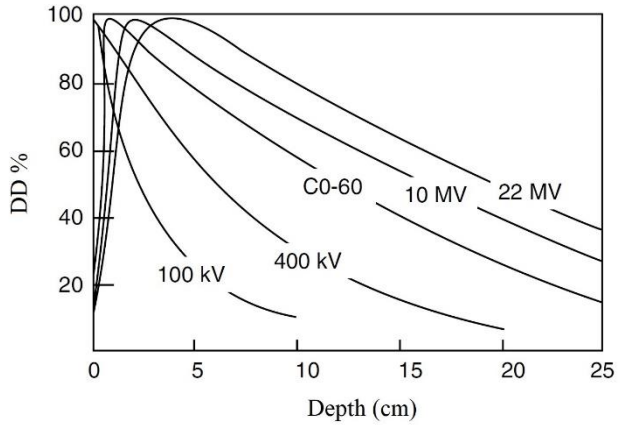

Figure 1.6 – PDD% curves for photons of different energies. Figure extracted from Beyzadeoglu *et al.* (2010) [4].

Given the interest of MV photon beams for RT, the *in vitro* radiosensitizer effect of AuNPs with MV has been investigated on various human tumour cell lines including breast, brain, colon, lung, and prostate [39,41,43–48]. Table 1.2 compiles the most recent studies, published since 2015, on irradiation of these cell lines assessed through clonogenic assays.

Wang *et al*. tested AuNPs with different sizes in the MDA-MB-231 breast cancer cell line irradiated with 6 MV. They obtained quite significant gains for both sizes: the 16 nm AuNPs conferred a gain of 1.49, while the larger AuNPs (49 nm) represented a 1.86-fold increase in cell death. Neither 16- nor 49 nm AuNPs induced remarkable cytotoxicity in the cell line. However, both size AuNPs induced G2/M arrest, which may justify the increased cell death obtained after RT with NPs. At last, 49 nm AuNPs produced greater G2/M arrest, which may be related to the fact that these NPs were more internalised by the cells [43]. Wolfe *et al*. tested two formulations of AuNPs (rod shape): one PEG-conjugated, and other PEG-goserelin-conjugated (a targeting ligand for prostate cancer). No significant gain was obtained with the AuNP-PEG, while AuNP-goserelin conferred a 1.35-fold increase in cell death [44]. This result emphasises the importance of the coating in the process of cellular internalisation of NPs and, consequently, in their potential for RT.

Saberi *et al*. irradiated the HT-29 colon cancer cell line using 9 MV X-rays and 50 nm AuNPs and obtained a gain of 1.4. Moreover, cell viability assays showed these AuNPs were not cytotoxic at different concentrations and incubation times. No cell cycle arrest in G2/M phase was detected after exposure to AuNPs. However, significant increase in apoptosis after RT+AuNPs compared to RT alone was observed [46]. Surprisingly, also for a colon cancer cell line (LOVO), the gain obtained by Hau *et al*. for 6 MV was superior to that for 50 kV: 35.2% *versus* 18.3%, respectively (*see* Table 1.1). Authors did not elaborate on the causes that may have led to this unexpected result [38].

Another colon cancer cell line (LS180) was tested by Zhang *et al*., who used two formulations of AuNPs: one PEG-conjugated, and other PEG-R8-conjugated (a cell-penetrating peptide which was shown to enhance drug delivery). While with the AuNP-PEG (20 nm) an insignificant gain of 1.07 was obtained, with AuNP-PEG-R8 (28 nm) a 1.36-fold increase in cell death was estimated. Again, this result emphasizes the importance of the coating in the process of cellular internalisation of NPs and, consequently, in their potential during RT. AuNPs cytotoxicity was also tested and neither AuNPs formulations reduced cell viability by more than 20% at concentrations up to 400 nM;

however, cell viability did appear to reduce in a concentration dependent manner. Furthermore, cell cycle, apoptosis, ROS levels and mitochondrial membrane potential were also analysed. AuNPs in combination with RT translated into an increased proportion of cells in G2/M phase, higher intracellular ROS levels, enhanced apoptosis, and a more significant impact on mitochondrial membrane depolarization, comparing to RT alone. As expected, AuNP-PEG-R8 showed more advantages for RT than the AuNP-PEG [47].

Kazmi *et al*. showed a considerable advantage of adding AuNPs to RT after irradiation of the U87 glioblastoma cell line with 6 MV and 42 nm AuNPs – a 1.45-fold increase in cell death. AuNPs cytotoxicity was also tested, and it was concluded that incubation with increasing concentrations of NPs for 3 and 24 h did not produce different cell viability levels [48]. Also using a glioblastoma cell line (U251), Liu *et al.* obtained a gain of 1.23 after irradiation with 6 MV and 15 nm AuNPs. The addition of AuNPs increased the radiation-induced apoptotic index as compared to RT alone. The cell viability assays showed that 24 h incubation with AuNPs alone caused a dose-dependent reduction of cell viability [45]. Finally, Tudda *et al*. tested irradiation of the MDA-MB-231 breast tumour cell line with 6 MV and 15 nm AuNPs. A gain of 1.04 was obtained than can be compared with the gain of 1.20 obtained for kV X-rays [41] (*see* Table 1.1). Also, Soleymanifard *et al.* obtained smaller gains after the irradiation with 6 MV beams than with kV. For MV and the same AuNPs, gains of just 32.4% and 39.3% were obtained for breast (MCF-7) and lung (QU-DB) cancer cell lines, respectively, compared to the ~64% gain obtained with kV X-rays [39] (*see* Table 1.1).

To the best of our knowledge, studies assessing the *in vitro* AuNPs potential for human pancreatic cancer cell lines irradiated with X-rays were not reported. Brero *et al.* tested 19.2 nm magnetic NPs (Fe_3O_4) and irradiated BxPC-3 cells with 6 MV and concluded that 50 μg/mL of these NPs conferred a 50-60% additive effect on cell death comparing to RT alone. NPs intrinsic cytotoxicity was also evaluated and a decrease in cell viability of only 3% was obtained after a 48-h incubation with NPs at different concentrations [49]. Detappe *et al.* evaluated 3.5 nm gadolinium-based NPs during irradiation with 220 kV of PANC-1 cells and concluded that 0.43 mg/mL of these NPs conferred a gain of 1.37 [MID(RT+NPs)/MID(RT)]. Furthermore, analyses of 53BP1 (protein with the same function as γH2AX) and apoptosis were performed – enhanced expression of radiation-induced 53BP1 *foci* and higher apoptosis were observed in irradiated groups previously incubated with NPs compared to RT alone [50]. Finally, the *in vivo* study by Yoshida *et al.* assessed the radiosensitization effect of 190 nm AuNPs microgels (AuNPs contents: 29.1 mg/mL, 100 μL) in mice injected with MIAPaCa-2 human pancreatic cancer cells and concluded that tumour growth was effectively suppressed in mice injected with AuNPs microgels when 150 kV X-rays irradiation was performed [51].

Table 1.2 – Summary of *in vitro* studies assessing AuNPs radiosensitization with 6 to 9 MV X-rays through clonogenic assays.

Author	Cell Line	X-rays (MV)	NP Size (nm)	Concentration	Gain factor	Model used
Tudda ***et al***. (2022)	MDA-MB-231 (Breast)	6	15	200 μg/mL	(1): 1.04 (2): 1.14	(1) $\frac{\text{MID (RT)}}{\text{MID (RT+NPs)}}$ (2) $\frac{D_{40\%}(\text{RT})}{D_{40\%}(\text{RT+NPs})}$
Kazmi ***et al***. (2020)	U87 (Brain)	6	42	100 μg/mL	1.45	$\frac{\text{SF2(RT)}}{\text{SF2(RT+NPs)}}$
Zhang ***et al***. (2018)	LS180 (Colon)	6	20 28	400 nM	1.07 1.36	SF2 was used. The model was not specified.
Saberi ***et al***. (2017)	HT-29 (Colon)	9	50	80 μM	1.4	$\frac{\text{MID (RT)}}{\text{MID (RT+NPs)}}$
Soleymanifard ***et al.*** (2017)	MCF-7 (Breast) QU-DB (Lung)	6	16	100 μM	39.3% 32.4%	$\frac{\text{SF2(RT)-SF2(RT+NPs)}}{\text{SF2(RT)}}$ (%)
Liu ***et al.*** (2016)	U251 (Brain)	6	15	50.76 μM	1.23	NR
Hau ***et al.*** (2016)	LOVO (Colon)	6	10	50 μg/mL	35.2%	NR
Wolfe ***et al.*** (2015)	PC3 (Prostate)	6	31	NR	(1): 1.09 1.35 (2): 1.19 1.36	(1) $\frac{D_{10\%}(\text{RT})}{D_{10\%}(\text{RT+NPs})}$ (2) $\frac{D_{20\%}(\text{RT})}{D_{20\%}(\text{RT+NPs})}$
Wang ***et al.*** (2015)	MDA-MB-231 (Breast)	6	16 49	20 nM	1.49 1.86	$\frac{\text{MID (RT)}}{\text{MID (RT+NPs)}}$

Abbreviations: MID = Mean Inactivation Dose, i.e., area under the survival curve; SFX = surviving fraction of cells irradiated with X Gy; $D_{X\%}$ = dose for which surviving fraction is X%; NPs = nanoparticles; RT = radiotherapy; NR = not reported.

Table 1.3 presents the most recent studies reporting the advantages of concomitant CRT *versus* RT alone for various human pancreatic cancer cell lines [52–56]. Depending on the cell line and drug concentration, among other factors, CRT gain factors ranged from 0.92 to 1.68. Despite these gain values, chemotherapy presents with several problems, such as the lack of drug-specific affinity towards the tumour, poor solubility and stability in physiological fluids, and nonspecific toxicity [16]. AuNPs have also been used to improve delivery of anticancer drugs during CRT – AuNPs present

with high surface area-to-volume ratio offering the possibility of applying various surface conjugations – a property useful for drug-delivery [16]. Due to their ability to be conjugated with anticancer drugs – such as gemcitabine, paclitaxel, and doxorubicin –, both biodistribution and locally deliver of anticancer drugs with reduced toxicity in healthy tissues can be improved [16]. However, as to the best of our knowledge, no studies involving AuNPs as a drug-delivery system combined with RT were found for pancreatic cancer.

Table 1.3 – Summary of *in vitro* studies assessing anticancer drugs radiosensitization for pancreatic cancer cells through clonogenic assay.

Author	Cell Line	Beam	Drug	Concentration(s)	Gain factor	Model used
Waissi ***et al.*** (2021)	BxPC-3 PANC-1 MIAPaCa-2 AsPc-1	^{137}C (γ-rays)	GEM	10 nM	BxPC-3: 1.75 PANC-1: 1.04 AsPC-1: 1.22 MIAPaCa-2: 1.04	$\frac{D_{10\%}(RT)}{D_{10\%}(RT+GEM)}$
Xu ***et al***. (2021)	PANC-1 SW1990	X-rays	DSF	15 μM	1.13 1.43	NR
Schwartz ***et al.*** (2020)	PANC-1 MIAPaCa-2	X-rays	CUR	6 μM 10 μM 12 μM	PANC-1: 1.06 1.53 1.93 MIAPaCa-2: 0.92 1.06 1.04	$\frac{D_{40\%}(RT)}{D_{40\%}(RT+CUR)}$
Tan ***et al***. (2020)	BxPC-3 Capan-2	6 MV X-rays	IBR	10 μM	1.34 1.68	$\frac{SF2(RT)}{SF2(RT+IBR)}$
Wang ***et al.*** (2020)	PANC-1 PaTu8988	X-rays	ROSI	40 μM	1.49 1.34	NR

Abbreviations: $D_{X\%}$ = dose for which surviving fraction is X%; SFX = surviving fraction of cells irradiated with X Gy; GEM = gemcitabine; DSF = Disulfiram; CUR = Curcumin; IBR = Ibrutinib; ROSI = Rosiglitazone; NR = not reported.

Clonogenic assays are well-established assays to investigate RT effects in cells survival [30], [57]. However, they can be very time-consuming in terms of post-irradiation incubation time – which can last weeks – and colony counting [58]. For the sake of this master dissertation, the 3-(4,5-dimethylthiazol-2-yl) 2,5-diphenyl tetrazolium bromide (MTT) assay was used to assess the effects produced by AuNPs in conjugation with RT, due to its multiple advantages: high reproducibility, rapid

semi-automated reading, and comparative low cost [57]. Therefore, a search on studies that relied on short-term assays (MTT assay or others) to evaluate the potential of AuNPs on human tumour cell lines irradiated with X-rays was also made (Table 1.4).

Shahhoseini *et al.* assessed the potential of 15 nm AuNPs during the irradiation of prostate (DU-145) and lung (A549) cancer cell lines with 6 MV X-rays. Cell viability was measured 24 or 48 h post-irradiation and AuNPs did not increase the cytotoxic effects of RT on either cell type. In addition, AuNPs alone did not induce loss of cell viability of both cell lines over 48 h and for various concentrations of AuNPs [59].

Also studying a prostate cancer cell line (DU-145), Zhang *et al.* tested two AuNPs formulations: a neutral one and other binding with glucose (to enhance cellular uptake). Both formulations produced a decrease in cell viability after 24 h incubation (13.52% and 17.82%, respectively); however, this decrease was not further accentuated after 48 and 72 h of incubation. Considering AuNPs effect on this cell line after irradiation with 200 kV X-rays, both formulations produced relevant inhibition rates on cell viability comparing to RT alone: 30.6% and 45.6%, for neutral and glucose-capped AuNPs, respectively [60].

Soleymanifard *et al.* obtained an enhancement of radiation toxicity caused by AuNPs of 19.8% and 15.7% for a lung cancer cell line (QU-DB), and 40.9% and 24.3% for a breast cancer cell line (MCF-7) after irradiation with 100 kV and 6 MV beams, respectively [39]. With the same breast tumour cells, Kong *et al*. obtained a cytotoxicity increase of about 63.5% with AuNPs 48 h post-irradiation comparing to RT alone [61].

To note that, in both studies, the gain added by AuNPs to RT assessed by the MTT assay was much lower than those obtained with clonogenic assays: 19.8% *versus* 64.4%; 15.7% *versus* 32.4%; 40.9% *versus* 64.1%; 24.3% *versus* 39.3%; and 63.5% *versus* complete cell death. This suggests that the MTT assay, despite its many practical advantages, may underestimate the true gain that might be obtained with concomitant RT with AuNPs.

Table 1.4 - Summary of *in vitro* studies assessing AuNPs radiosensitization with X-rays through MTT assay.

Author	Cell Line	X-rays	NP Size (nm)	Concentration	Gain factor	Model used
Shahhoseini ***et al.*** (2019)	DU-145 (Prostate)	6 MV	15	1 mM	0	NA
	A549 (Lung)				0	
Soleymanifard ***et al.*** (2017)	MCF-7 (Breast)	100 kV 6 MV	16	100 μM	40.9% 24.3%	$\frac{CV(RT)-CV(RT+NPs)}{CV(RT)}$ (%)
	QU-DB (Lung)				19.8% 15.7%	
Kong ***et al.*** (2008)	MCF-7 (Breast)	200 kV	11	15 nM	63.5%	$\frac{CV(RT)-CV(RT+NPs)}{CV(RT)}$ (%)
Zhang ***et al.*** (2008)	DU-145 (Prostate)	200 kV	7	15 nM	30.6% 45.6%	NR

Abbreviations: NA = not applicable; CV = cell viability (%); RT = radiotherapy; NPs = nanoparticles; NR = not reported.

2. Materials and Methods

2.1. Cell line culture conditions

Human pancreatic adenocarcinoma BxPC-3 (ATCC© CRL-1687™) cells were cultured in RPMI-1640, supplemented with 10% fetal bovine serum and 100 IU/mL of penicillin and 100 µg/mL streptomycin (Gibco, Thermo Fisher Scientific, Waltham, MA, USA), further designated as complete medium. Cells were kept at 37 °C, under a 5% CO_2 atmosphere. Maintenance of cultures was performed every 2-3 days, until cells reached a confluence of about 80%.

2.2. Synthesis of HAOA-AuNPs and BBN-AuNPs

HAOA-AuNPs were donated by Faculdade de Farmácia da Universidade de Lisboa (FFUL) and prepared as previously described in [22]. Gold (III) chloride trihydrate ($HAuCl_4 \cdot 3H_2O$), silver nitrate (A_gNO_3), L-ascorbic acid (L-AA), aqueous solution containing 5.9% of rosmarinic acid, hyaluronic acid (HA) from *Streptococcus Equi* (MW ~1.5–1.8 x 10^6 Da), and oleic acid (OA; MW = 282.46 g/mol) were supplied from Sigma-Aldrich (Steinheim, Germany), as reported [62]. Briefly, fresh solutions of gold salt, silver nitrate, L-ascorbic acid and an aqueous solution containing 5.9% of rosmarinic acid were prepared. The coating was previously prepared by mixing HA and OA, followed by stirring the suspension overnight at 400 rpm at 60 °C. The reaction of preparing uncoated AuNPs was carried out at 800 rpm for 15 min in a stirring plate (Fisherbrand ARE Hotplate Stirrer, Bradford, UK). On the next day, the coating suspension (HAOA) was added to the AuNPs core (proportion 1:1, *v/v*) and stirred for 30 min at 800 rpm at room temperature. Finally, HAOA-AuNPs were centrifuged and stored at 4 °C, protected from the light [62].

BBN-AuNPs were donated by Ciências Radiofarmacêuticas Group of C2TN/IST and prepared as previously described in [63]. Firstly, AuNPs stabilized with 2-[4,7-bis(carboxymethyl)-10-[2-(3-sulfanylpropanoylamino) ethyl]- 1,4,7,10-tetrazacyclododec-1-yl] acetic acid (TDOTA) were synthetized. The final solution was centrifuged at 1000 rpm for 20 min and the pellet obtained was washed two times with methanol (MeOH) and two times with H_2O. NPs were then dried at reduced pressure. Thioctic acid terminated bombesin peptide (SS-BBN) was prepared in an automated peptide synthesizer. The final product was prepared by mixing AuNP-TDOTA with the thiolated peptide in a 1:2 ratio (*w/w*) at room temperature for 2 h. Briefly, 800 µL of MeOH were added to a 200 µL suspension of AuNP-TDOTA (5 mg/mL in deionized water) and then 1 mL of a solution of SS-BBN (2 mg, 1.77 µmol, in MeOH) was added. The mixtures were stirred at room temperature for 2 h. Then, centrifugation at 12000 rpm for 5 min was performed. The BBN-AuNPs were washed with MeOH and H_2O and dried at low pressure [63].

2.3. Characterization of HAOA-AuNPs and BBN-AuNPs

AuNPs were characterized in terms of mean particle size and polydispersity index (PdI) [HAOA-AuNPs diluted in phosphate buffered saline (PBS) and BBN-AuNPs diluted in de-ionized water, 1:10] through Dynamic Light Scattering (DLS) (Zetasizer Nano S; Malvern Instruments, Malvern, UK).

AuNPs were also characterized in terms of morphology and mean particle size by Atomic Force Microscopy (AFM). Briefly, 40 µL of each sample was placed on a freshly cleaved mica surface and allowed to dry for one hour before analysis. Images were acquired by Multimode 8 HR coupled to Nanoscope V Controller (Bruker, Coventry, UK), using a peak force tapping and ScanAssist mode. Tip model used was scanasyst-air 0.4 N/m, Bruker.

2.4. Irradiation setup and cells irradiation

The planning target volume for pancreatic tumours is usually located at a depth ranging between 5 to 20 cm. Thus, to mimic as much as possible the location of this target, a phantom allowing the irradiation of the BxPC-3 cells layer at a depth of 10 cm was build. The phantom was composed by a stack of 9 polystyrene plates (ρ = 1.045 g/cm^3) of 30 x 30 x 1 cm; a set of polymethylmethacrylate (PMMA) plates (ρ = 1.19 g/cm^3) – 1 plate of 30 x 30 x 0.6 cm + 16 small plates mounted around the 96-well plate (4 plates mounted in each side totalling a thickness of 1.75cm – *see* Figure 2.1, b) –, and five plates of polystyrene on top of the 96-well plate to guarantee full backscatter radiation (Figure 2.1). polystyrene plates belonged to the Champalimaud Foundation (Lisbon, Portugal). PMMA plates were designed and acquired for this study to accommodate the 96-well plates used for BxPC-3 cells irradiation to avoid the presence of air around it. Air cavities provide localized regions of low-density which lead to variations between the planned dose and the delivered dose.

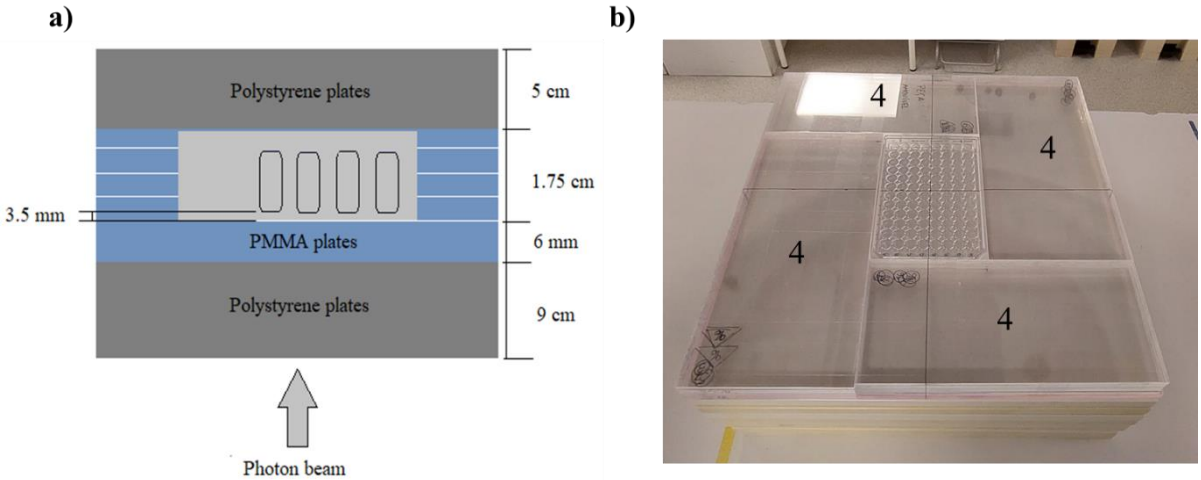

Figure 2.1 – (a) Schematic representation of the phantom used for cell irradiation (axial cut). The polystyrene plates (dark grey) in conjugation with the PMMA plates (blue) allowed irradiation of a 96-well plate (light grey) positioning the cells at a depth of 10 cm. The image is not to scale. (b) The 16 small PMMA plates mounted around the 96-well plate – 4 plates mounted in each side totalling a thickness of 1.75cm.

For treatment planning, a CT of this phantom (Figure 2.2) was acquired using a Philips Brilliance Big Bore 16 Slice CT Simulator (Koninklijke Philips N.V.). Treatment planning (Figure 2.3) was made by Dr Sandra Vieira in the treatment planning system Eclipse (Eclipse Software, Varian Medical Systems, Inc.).

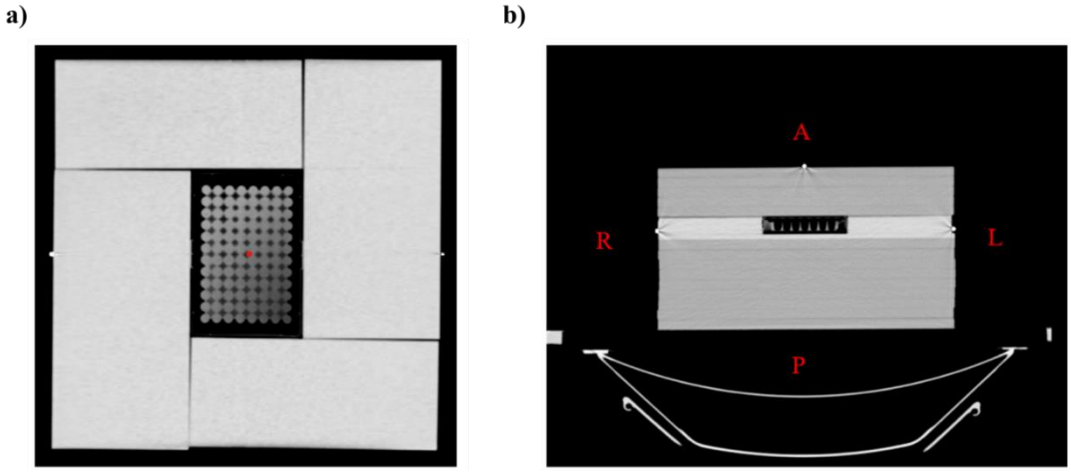

Figure 2.2 – CT of the phantom used for irradiation of BxPC-3 cells in a 96-well plate: (a) a coronal plane with representation of the isocentre (red dot), (b) an axial plane with representation of posterior (P), anterior (A), right (R), and left (L) sides.

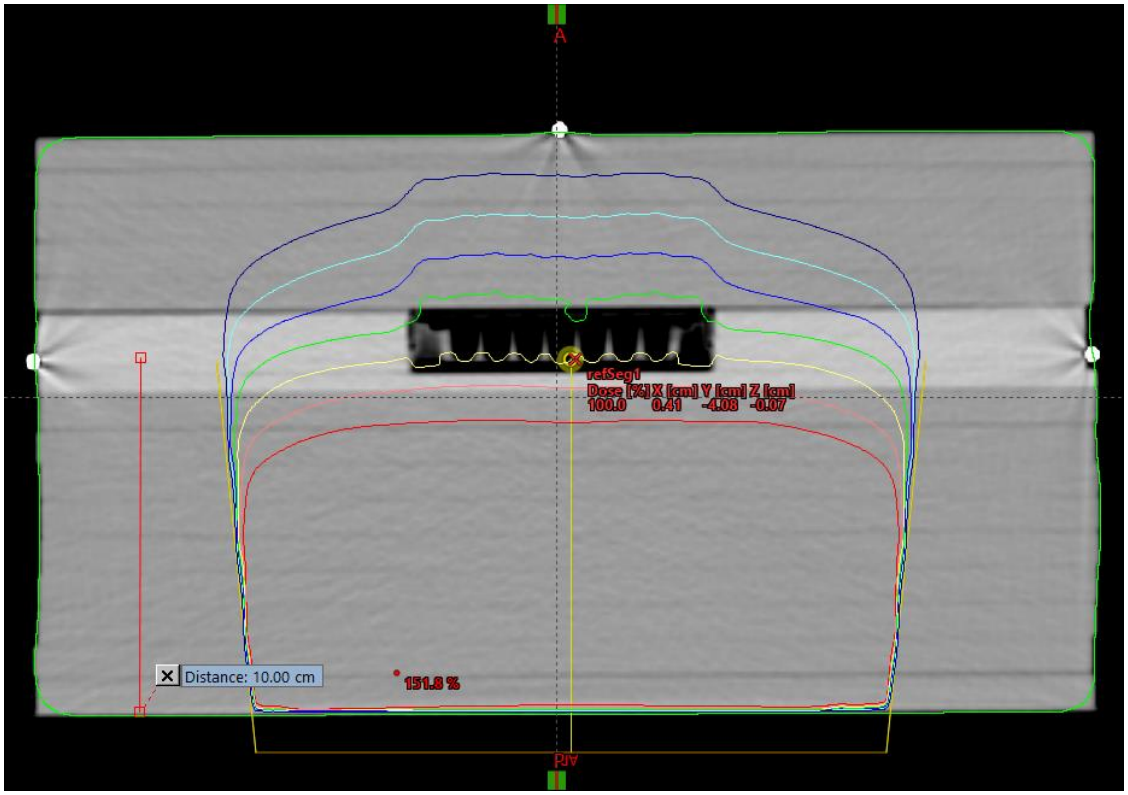

Figure 2.3 – RT plan showing the planned dose distribution by a 20x20 cm^2 6 MV field size. Treatment planning was performed to deliver 100 % of each radiation dose with a posteroanterior (PA) beam at a 10 cm depth.

Before irradiation, BxPC-3 cells were trypsinized and suspensions at the appropriate cell concentration were prepared. Cells were seeded in 96-well plates (200 μL) and allowed to adhere for 24 h. After this time, supernatant was discarded, and cells were incubated with AuNPs for 4 h to allow internalization. Then, supernatant was discarded, and 100 μL of complete medium was added to each well. The 96-well plates were transported to Champalimaud Foundation (Lisbon, Portugal) inside a Styrofoam box with closed containers of hot water inside. This minimized the possible stress caused by temperature variations.

For irradiation, all BxPC-3 cell plates were placed inside the phantom at a depth of 10 cm at the isocentre of a Varian Edge medical LINAC (Varian Medical Systems, Inc., Palo Alto, CA, USA) (Figure 2.4). Irradiation was performed with a 6 MV posteroanterior (PA) uniform beam, produced by a standard flattening filter, with a 20 × 20 cm^2 field size, unless stated otherwise. A PA beam was used to avoid the beam from having to pass through air before reaching the cells. Depending on the test, cells were irradiated with different radiation doses ranging from 2 to 10 Gy at a dose rate of 600 MU/min. Radiation exposures were conducted at room temperature. As most of cell experiments were performed using this irradiation setup, this plan will be name throughout the text as the standard plan configuration.

After irradiation, BxPC-3 cell plates were transported back to the laboratory, and 100 μL of complete medium was added to each well following incubation at the above specified conditions during the pre-selected period times for viability assays evaluation. Total travelling time to and back from the Champalimaud Foundation was about 2 - 3 h.

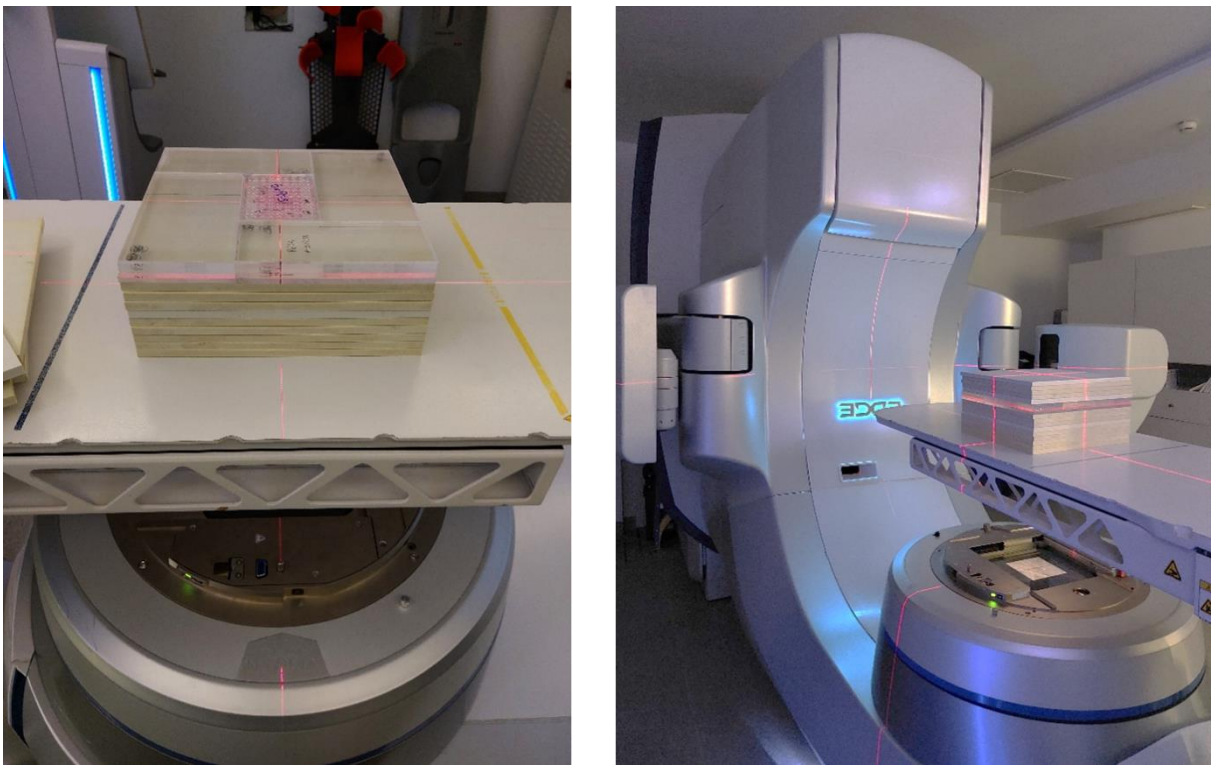

Figure 2.4 – Irradiation set-up. Each well plate was placed inside the phantom in such a way that cells were at a depth of 10 cm when irradiated with a 6 MV posterior beam (gantry position at 180º).

2.5. Cell viability by MTT assay

In this exploratory study, MTT assay – a colorimetric short-term *in vitro* assay – was used. This assay is based on the reduction of the soluble yellow tetrazolium salt (MTT) by dehydrogenases in mitochondria or endoplasmic reticulum to water-insoluble dark-coloured formazan crystals by metabolically active cells [26,30,58]. After crystal solubilisation with a solvent, the lowering of the light transmission by the homogenized MTT-formazan solution is measured in terms of its absorbance by a microplate reader at a wavelength which MTT-derived formazan absorbs the most (around 570 nm) [26].

The viability of BxPC-3 cells after irradiation and incubation at pre-selected times was evaluated by MTT assay. Briefly, medium was discarded following twice washing with PBS, and 50 μL of MTT reagent at a concentration of 0.5 mg/mL in incomplete medium were added to each well. Following an incubation period of 2 - 4 h, 100 μL of dimethyl sulfoxide (DMSO) were added to each well to solubilize the formazan crystals. After solubilisation, absorbance was measured at 570 nm in a microplate reader (BioTek ELx800; BioTek Instruments, Inc.,Winooski, VT, USA). Cell plates transported to Champalimaud Foundation but not irradiated neither incubated with AuNPs were defined as the control group and were assigned a value to a value of 100% of cell viability. Results of the test groups (RT alone, AuNPs alone, and RT + AuNPs) were normalized to the control, i.e., cell viability (%) was calculated based on the following expression:

$$\text{Cell Viability (\%)} = \frac{\text{Absorbance (test group)}}{\text{Absorbance (control group)}} \times 100\%$$

(Equation 2.1)

2.6. Impact of transport on cell viability

BxPC-3 cell plates were transported by car to Champalimaud Foundation, accommodated inside a box, as previously described. To assess how transport influenced cell viability, BxPC-3 cells were seeded in 96-well plates (200 μL) at different concentrations (1×10^4, 2×10^4, and 4×10^4 cells/mL) and allowed to adhere for 24 h. Then, medium was discarded, and 100 μL of complete medium was added to each well. One plate stayed in the laboratory incubator (control group), and another one was transported to Champalimaud Foundation but not irradiated and brought back to incubator after 2 – 3 h. Cell viability was evaluated by the MTT assay 24 and 48 h after transport.

2.7. Influence of cell concentration

Aiming to establish the best MTT assay conditions for subsequent assays, the influence of cell concentration on cell viability results was tested. Succinctly, BxPC-3 cells were seeded in 96-well plates (200 μL) at different concentrations:1×10^4, 2×10^4, and 4×10^4 cells/mL, and allowed to adhere for 24 h. Then, medium was discarded, and 100 μL of complete medium was added to each well. Cells were irradiated using the standard setup configuration with 2 and 8 Gy. Cell viability was evaluated by MTT assay 24 and 48 h post-irradiation.

2.8. Influence of incubation time after irradiation

To validate the best MTT assay conditions for the subsequent assays (with AuNPs), the influence of different incubation times post-irradiation on cell viability was tested. Succinctly, BxPC-3 cells were seeded in 96-well plates (200 μL) at 4×10^4 cells/mL and allowed to adhere for 24 h. Then, medium was discarded, and 100 μL of complete medium was added to each well. Cells were irradiated using the standard setup configuration with 2, 5, and 10 Gy. Cell viability was evaluated by MTT assay 24, 48, and 72 h post-irradiation.

2.9. AuNPs cytotoxicity on BxPC-3 cell line

To assess the effect of HAOA-AuNPs and BBN-AuNPs on cell proliferation, BxPC-3 cells were incubated with AuNPs at different concentrations in terms of gold content: 50, 200, and 400 μM. Briefly, cells were seeded in 96-well plates (200 μL) at a density of 5×10^4 cells/mL and allowed to adhere for 24 h. After this time, complete medium was discarded, and cells were incubated for 24 and 48 h with AuNPs. After this time, medium was discarded and MTT assay was performed as described in section 2.5.

For simplicity, from now on, the 'gold concentration present in AuNPs' will sometimes be indicated as just 'AuNPs concentration', i.e., 50 μM of AuNPs corresponds to AuNPs with 50 μM in terms of gold content.

2.10. Impact of HAOA-AuNPs during RT

To investigate the impact of concomitant RT with HAOA-AuNPs, BxPC-3 cells were incubated with these NPs at different gold concentrations (50, 200, and 400 μM). Briefly, cells were seeded in 96-well plates (200 μL) at 4×10^4 cells/mL and allowed to adhere for 24 h. After this time, complete medium was discarded, and cells were in contact with HAOA-AuNPs for 4 h to allow internalization. Afterwards, AuNPs were discarded, and 100 μL of complete medium was added to each well. Cells were irradiated using the standard setup with 2, 3.5, and 5 Gy. After irradiation, 100 μL of complete medium was added to each well and cells were incubated for 48 and 72 h. Then, cell viability was evaluated by MTT assay.

2.11. Impact of size and coating: BBN-AuNPs during RT

With the purpose of evaluating the impact of AuNPs with a different size and coating during RT, BxPC-3 cells were incubated with BBN-AuNPs at 50 and 200 μM in terms of gold content. Briefly, cells were seeded in 96-well plates (200 μL) at 4×10^4 cells/mL and allowed to adhere for 24 h. After this time, complete medium was discarded, and cells were in contact with BBN-AuNPs for 4 h to allow internalization. Afterwards, AuNPs were discarded, and 100 μL of complete medium was added to each well. Cells were irradiated using the standard setup configuration with 2, 3.5, and 5 Gy.

After irradiation, 100 μL of complete medium was added to each well and cells were incubated for 48 and 72 h. Then, cell viability was evaluated by MTT assay.

2.12. Impact of field size during RT with AuNPs

To investigate the impact of field size during RT with AuNPs, BxPC-3 cells were incubated with HAOA-AuNPs at 50, 100, and 200 μM in terms of gold content. Briefly, cells were seeded in 96-well plates (200 μL) at 4×10^4 cells/mL and allowed to adhere for 24 h. After this time, complete medium was discarded, and cells were in contact with HAOA-AuNPs for 4 h to allow internalization. Afterwards, AuNPs were discarded, and 100 μL of complete medium was added to each well. Cells were irradiated with 2 Gy delivered by a posterior 6 MV beam for the field sizes: 8x8, 20x20, and 30x30 cm^2. After irradiation, 100 μL of complete medium was added to each well and cells were incubated for 72 h. Then, cell viability was evaluated by MTT assay.

2.13. Impact of free-flattening filter beam during RT with AuNPs

To investigate the impact of beam spectra originating from a free-flattening filter (FFF) LINAC during RT with AuNPs, BxPC-3 cells were incubated with HAOA-AuNPs at 200 μM in terms of gold content. Briefly, cells were seeded in 96-well plates (200 μL) at 4×10^4 cells/mL and allowed to adhere for 24 h. After this time, complete medium was discarded, and cells were in contact with HAOA-AuNPs for 4 h to allow internalization. Afterwards, AuNPs were discarded, and 100 μL of complete medium was added to each well. Cells were irradiated with 2 Gy using a posterior 6 MV beam delivered without flattening filter for a 20x20 cm^2 field size. After irradiation, 100 μL of complete medium was added to each well and cells were incubated for 72 h. Cell viability was evaluated by the MTT assay.

2.14. Dosimetry

In this master thesis, most cells irradiations were performed with a setup configuration using a 6 MV beam of 20x20 cm^2 at a 10 cm depth (standard setup) and here named as Plan 1, whose planned dose distribution can be seen in Figure 2.5, a. Because no dose measurements were made, to assess if cells within the 96-well plate were being homogeneously irradiated, a dosimetric analysis of the dose distribution at the irradiation depth was performed based on the calculated doses by the treatment planning system. Thus, these planned doses were exported from Eclipse (Eclipse Software, Varian Medical Systems, Inc., Palo Alto, CA, USA) and imported for analysis in 3D Slicer version 5.0.2. The CT slice at the depth of the isocentre was chosen and a region of interest was defined for each well with a diameter slightly smaller than the well diameter. The average dose of each region of interest was collected for analysis.

Irradiation time at a clinical LINAC is limited and cell irradiation using the standard irradiation setup is quite time-consuming and expensive. Thus, to optimize cells irradiation in future studies, plans using multiple segments allowing the delivery of various radiation doses to each 96-well

plate were tested. This approach was successfully tested with IMRT by others [64]. However, to perform this type of irradiation with accuracy, RT planning and delivery is quite complex. Thus, to simplify the delivery, two new plans were made. Plan 2 was based on the delivery of two segments, i.e., the first segment was a 20x20 cm^2 field delivering 2 Gy and the second segment was a semi-field delivering 1.5 Gy. Thus, this plan allows the irradiation of cells with two radiation doses: 2 and 3.5 Gy. The total dose distribution delivered by this plan can be seen in Figure 2.5, b). Plan 3 was composed by three segments, i.e., the first segment was a 20x20 cm^2 field delivering 2 Gy, the second segment was an asymmetric field of 11.8x20 cm^2 delivering 1.5 Gy, and the third segment was an asymmetric field of 8.2x20 cm^2 delivering 1.5 Gy. The total dose distribution of Plan 3 can be seen in Figure 2.5, c). Similarly, the planned dose distribution was exported from Eclipse and imported for analysis in 3D Slicer.

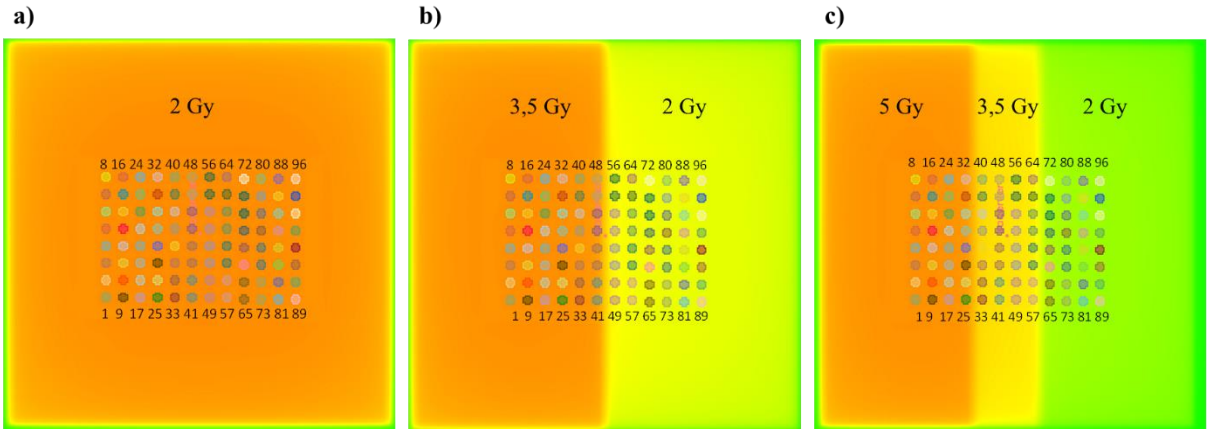

Figure 2.5 – Dose distribution for (a) Plan 1, (b) Plan 2 and (c) Plan 3 based on the irradiation of a single segment, two segments and three segments, respectively.

2.15. Statistical analysis

Cell viability measurements of BxPC-3 cells were presented as the mean ± standard deviation (SD). All data analysis was performed using GraphPad Prism version 9.4.0 (GraphPad Software, Inc., San Diego, CA, USA) and a p-value < 0.05 was considered as statistically significant. Impact of transport on cell viability was evaluated by multiple t-test using the Holm-Šídák method. Impact of free-flattening filter during RT with HAOA-AuNPs was assessed by two-way ANOVA followed by Šídák's multiple comparisons test. The other assays regarding cell viability were evaluated by two-way ANOVA followed by Tukey's multiple comparisons test. All the results of the statistical analysis can be found in the Appendix.

3. Results and Discussion

3.1. Characterization of HAOA-AuNPs and BBN-AuNPs

Both AuNPs used in the present work were evaluated in terms of their mean particle size by DLS and AFM (Table 3.1) and in terms of their morphology by AFM. By DLS, a mean particle size of 118 nm and 960 nm was obtained for HAOA-AuNPs (PdI < 0.3) and BBN-AuNPs (PdI > 0.4), respectively. AFM technique demonstrated that both AuNPs presented a spherical morphology (Figure 3.1) with a mean particle size of 119 nm and 47 nm for HAOA-AuNPs and BBN-AuNPs, respectively.

Table 3.1 – Mean particle size of HAOA-AuNPs and BBN-AuNPs. Data are presented as mean value ± SD, *n* = 3.

AuNPs Formulation	Mean size (nm) (DLS)	PdI	Mean size (nm) (AFM)
HAOA-AuNPs	118 ± 7	0.202 ± 0.013	119 ± 28
BBN-AuNPs	960 ± 59	0.489 ± 0.093	47 ± 8

Abbreviations: HAOA-AuNPs = gold nanoparticles coated with hyaluronic and oleic acids; BBN-AuNPs = gold nanoparticles coated with bombesin; DLS = Dynamic Light Scattering; PdI = polydispersity index; AFM = Atomic Force Microscopy.

The HAOA-AuNP size based on the AFM technique confirmed the results obtained by DLS. However, for BBN-AuNPs, results from both techniques were not concordant. A mean particle size of 960 nm for these AuNPs may be associated with the presence of aggregates. Indeed, the high PdI value obtained indicates the high heterogeneity of the AuNPs suspension used in the present work.

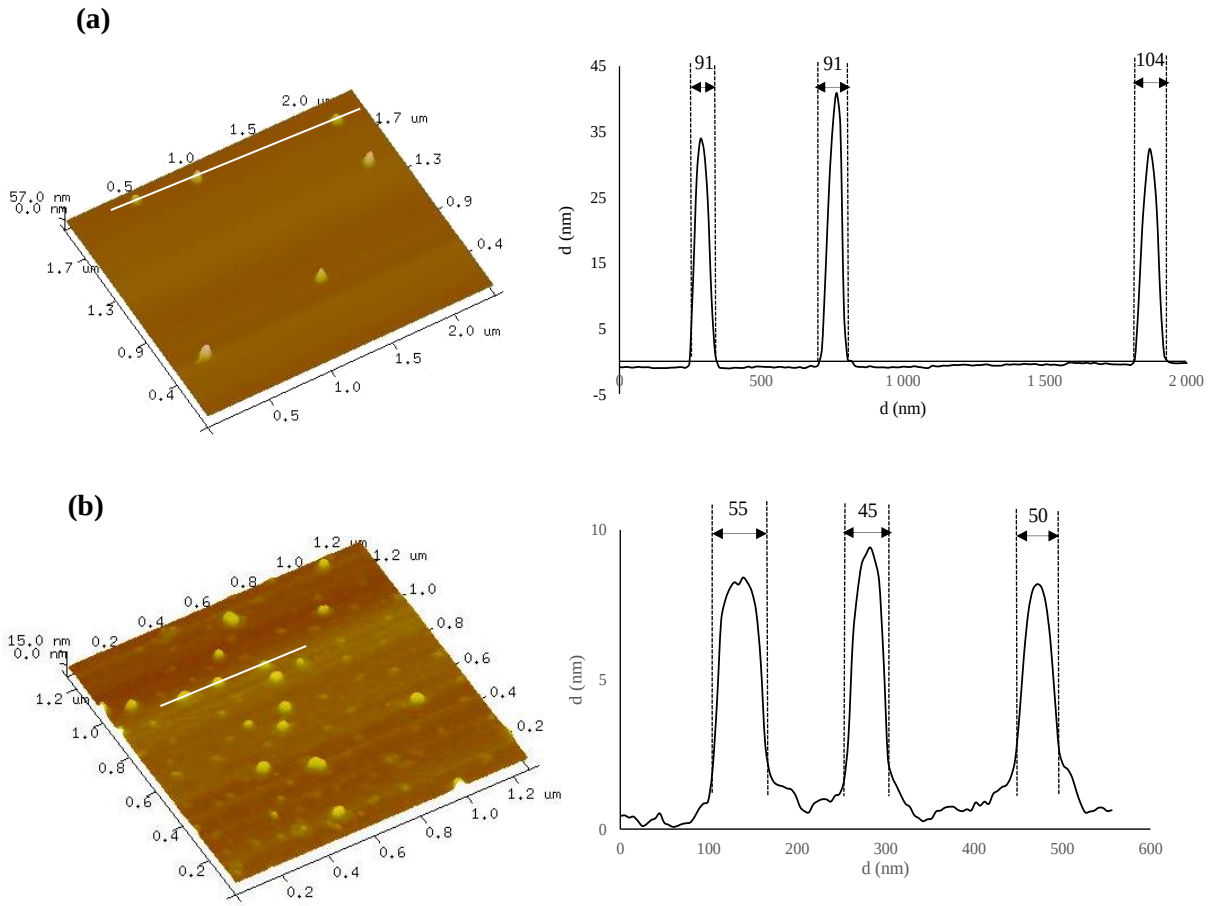

Figure 3.1 – 3D Atomic Force Microscopy (AFM) images with corresponding cross-section profiles of two different AuNPs formulations: (a) HAOA-AuNPs and (b) BBN-AuNPs.

3.2. Impact of transport on cell viability

The transport of the BxPC-3 cell plates was done under conditions that aimed to maintain as much as possible the temperature conditions present during incubation. However, to perform irradiation, the cell plates had to be removed from the Styrofoam box where they were accommodated during travelling. In total, from the time they were placed in the container for transport until they returned to the laboratory after irradiation, cells were out of the incubator for 2 – 3 h. Thus, aiming to know the impact that transport had on cell viability and to define whether the control for subsequent assays should also be transported, increasing cell concentrations ranging from 1×10^4 to 4×10^4 cells/mL were used. A cell viability comparison between cells that were kept in the incubator and cells that were transported was assessed by MTT assay 24 and 48 h after transport. Results are presented in Figure 3.2.

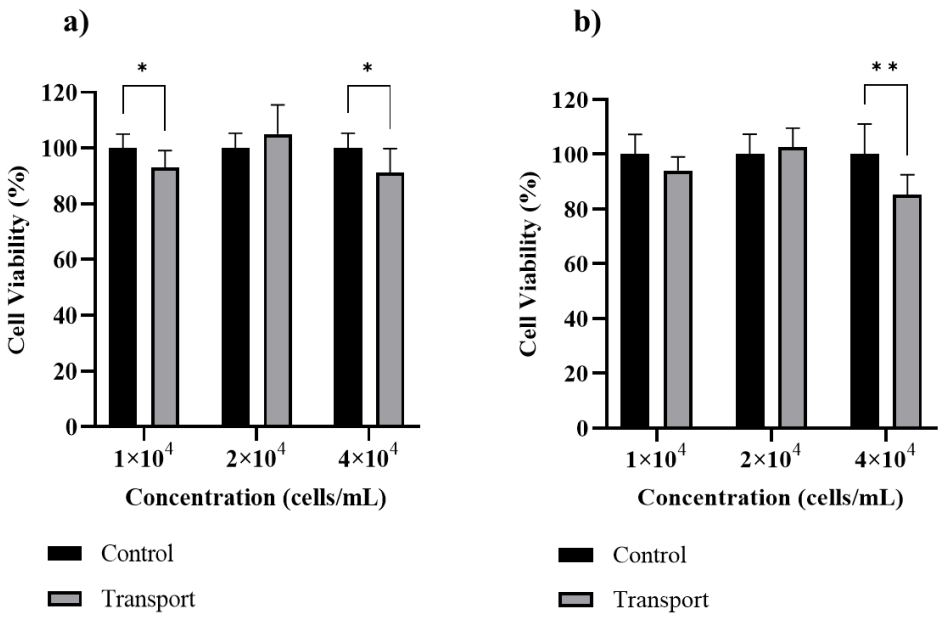

Figure 3.2 - Cell viability (%) of BxPC-3 cells (a) 24 h and (b) 48 h after being transported to the local of irradiations. *p < 0.05, **p < 0.01. Data are presented as mean value ± SD, *n* = 1.

For the lower cell concentration tested, cell viability of transported cells after 24 h was significantly different (p = 0.02) compared to control; however, a loss in cell viability < 10% was obtained. Nevertheless, for this cell concentration, no significant differences (p = 0.07) were observed for the 48-h incubation period.

For the cell concentration of 2×10^4 cells/mL, no statistically significant changes between control and transport were observed for both incubation periods (p > 0.05). For the higher cell concentration, statistically significant differences in cell viability of approximately 9 and 15 %, for the 24 and 48 h incubation periods after transport were observed, respectively (p = 0.02; p = 0.005).

A cell viability loss was particularly observed at the highest cell concentration tested. At this experimental condition, there is a higher cell density, which could facilitate their detachment from the bottom of the wells leading to cell death. Based on these results, it was defined that one plate should always be transported along with all the tested plates, constituting the control group.

3.3. Influence of cell concentration

Initial studies were carried out to establish the best conditions to perform MTT assays. Thus, it was tested the influence of cell concentration when BxPC-3 cells were irradiated with 2 and 8 Gy. The cell viability of irradiated and non-irradiated cell cultures, using increasing cell concentrations ranging from 1×10^4 to 4×10^4 cells/mL, was assessed using the MTT assay 24 and 48 h post-irradiation. Results are presented in Figure 3.3.

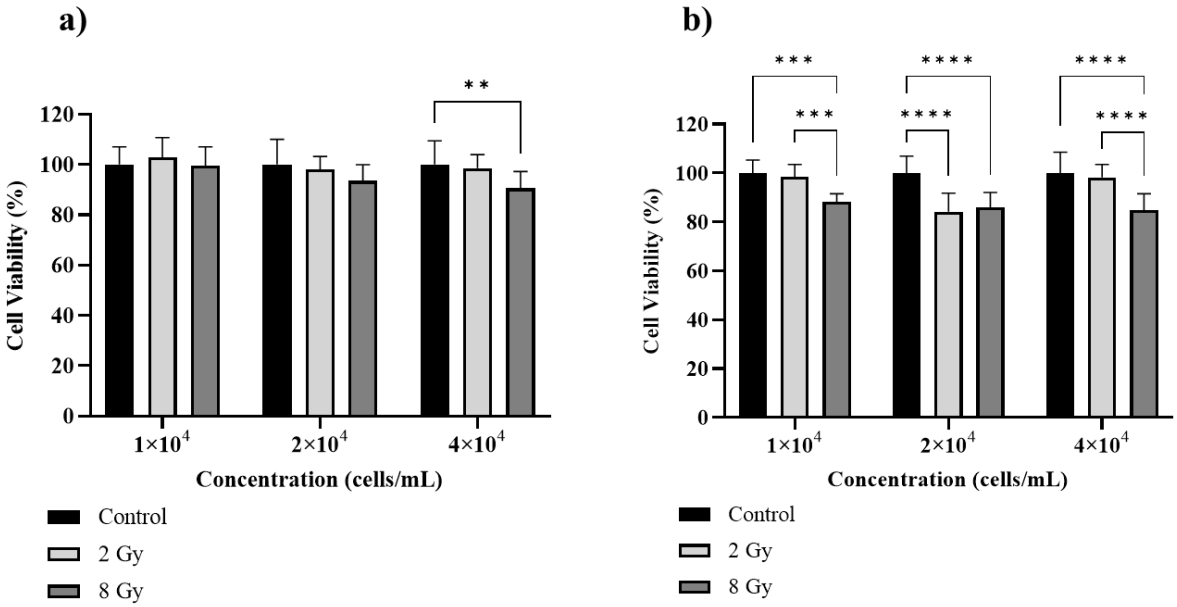

Figure 3.3 - Cell viability (%) of BxPC-3 cell line (a) 24 h and (b) 48 h after different cell concentrations were irradiated with 2 and 8 Gy. **p < 0.01, ***p < 0.001, ****p < 0.0001. Data are presented as mean value ± SD, $n = 1$.

At 24 h after irradiation, a statistically significant decrease in cell viability (< 10%) was obtained only for the highest cell concentration group, after irradiation with 8 Gy ($p = 0.008$). Considering the 48-h incubation period, irradiation with 2 Gy led to a statistically significant decrease in cell viability of about 16% for the intermediate cell concentration when compared with the control ($p < 0.0001$). For the other cell concentrations, no variations in cell viability were obtained under these conditions. However, for cells irradiated with 8 Gy, significant cell viability losses were observed for all cell concentrations: 12%, 14%, and 15%, respectively, when compared with control ($p \leq 0.0001$).

In summary, the highest cell concentration was the experimental condition that allowed to achieve more accentuated differences between the control and cells irradiated with 8 Gy for both post-irradiation incubation times. Thus, this cell concentration was set for subsequent assays.

3.4. Influence of incubation time after irradiation

The influence of radiation dose on cell viability was assessed 24, 48, and 72 h post-irradiation by MTT assay. Three different radiation doses were tested: 2, 5, and 10 Gy. Results are presented in Figure 3.4.

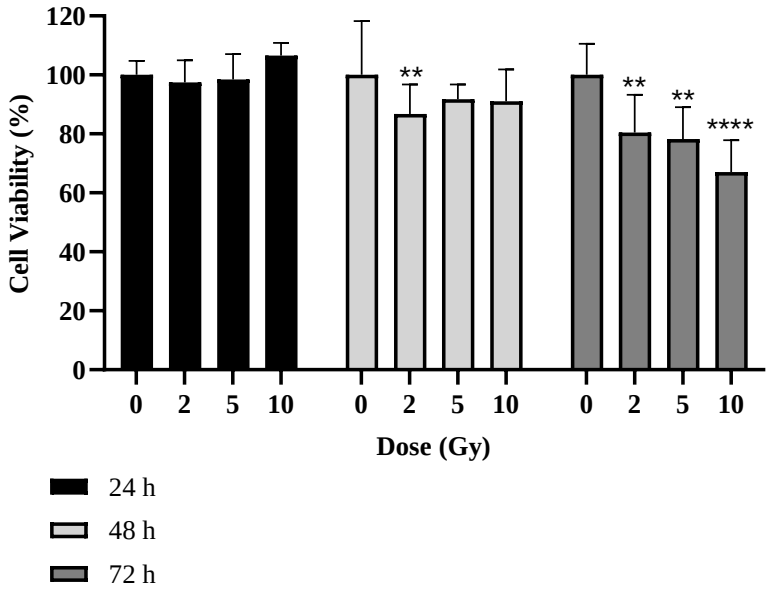

Figure 3.4 - Cell viability (%) of BxPC-3 cell line 24, 48, and 72 h after irradiation with 2, 5, and 10 Gy. **p < 0.01, ****p < 0.0001 compared to control (0 Gy) in the same post-irradiation incubation time. Data are presented as mean value ± SD, *n* = 1.

For the 24-h post-irradiation time, no significant differences were noted between the control and groups of cells irradiated. For the 48-h post-irradiation time, statistically significant differences were only obtained for cells irradiated with 2 Gy: < 13% when comparing to control group (p = 0.002). On the other hand, neither 5 Gy nor 10 Gy led to a loss in cell viability. Similarly, Kong *et al.* did not obtain a reduction in cell viability of the human breast cancer cell line (MCF-7) 48 h following irradiation with 10 Gy. Indeed, the authors reported a 11.5% increase on cell viability when compared to control [61].

For the 72-h post-irradiation time, statistically significant decreases in cell viability of about 20%, 22%, and 33% were obtained after irradiation with 2, 5, and 10 Gy, respectively (p = 0.004; p = 0.001; p < 0.0001). Masoudi-Khoram *et al.* obtained similar results after irradiation of the human breast tumour cell line (MDA-MB-231). Significant reductions in cell viability were only observed 72 h following irradiation with 6 and 10 Gy when compared to control [65].

As the highest differences in cell viability between irradiated and control groups were observed for the 72-h post-irradiation time, this experimental condition was selected as the most appropriate for further assays. One of the possible reasons why such differences in terms of cell viability were not observed for the 24 and 48 h incubation periods might be due to the lag period of cells after irradiation. This delay is probably due to the time frame of cell death following irradiation,

related to damage repair being also cell-line dependent [57]. If cell viability is measured during the lag phase (i.e., too early), survival is overestimated. For BxPC-3 cells, used in the present work, the doubling time is 48 - 60h [66]. Thus, for incubation times lower than this period, cell survival may be overestimated. Furthermore, the lag period is also influenced by the radiation dose – increasing RT doses lead to an increase lag period and, consequently, to a need to increase incubation time post-irradiation to accurately observe the losses in cell viability (*see* Figure 6.2 in Appendix) [57]. Unfortunately, increasing incubation time to counteract this effect may not be feasible as overpopulation of the cells is quite likely to occur for long incubation times inside the small wells. Also, in the typical MTT assay there are no medium changes which can possibly lead to a shortage of nutrients for the cells.

3.5. AuNPs cytotoxicity on BxPC-3 cell line

To perform cell viability assays that aimed to evaluate the effects of RT in conjunction with AuNPs, an evaluation of the cytotoxic effect that AuNPs alone induced in BxPC-3 cells was made. Thus, the cytotoxicity of HAOA-AuNPs and BBN-AuNPs was assessed by MTT assay after a 24- and 48-h incubation times with concentrations ranging from 50 to 400 μM. Results are presented in Figure 3.5, a) for HAOA-AuNPs and Figure 3.5, b) for BBN-AuNPs.

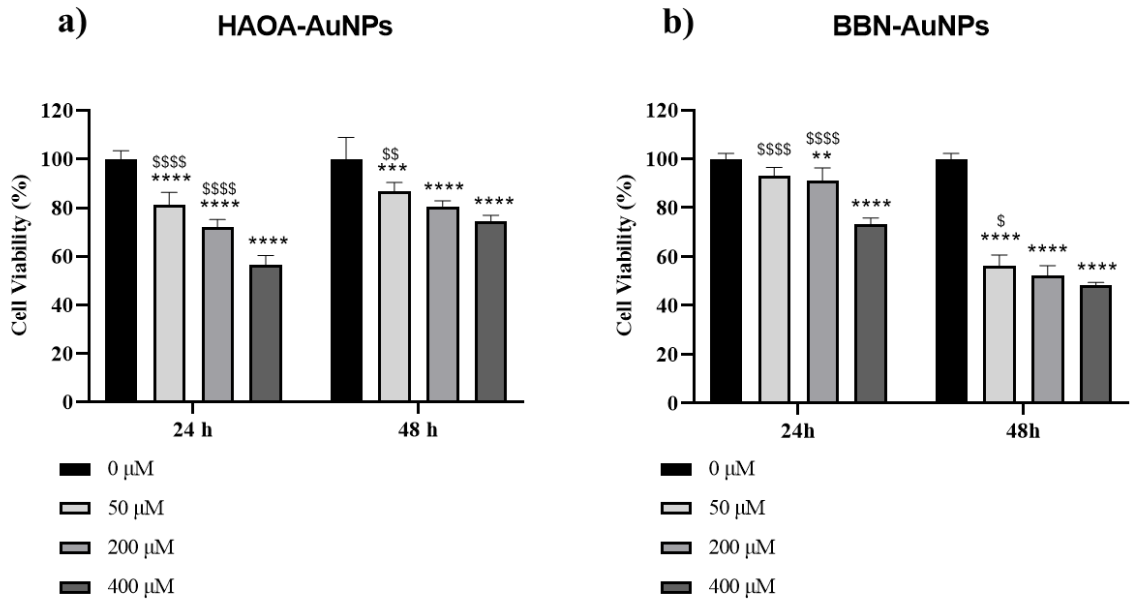

Figure 3.5 - Cell viability (%) of BxPC-3 cell line 24 and 48 h after incubation with 50, 200, and 400 μM of (a) HAOA-AuNPs and (b) BBN-AuNPs. **** $p < 0.0001$ comparing to control (0 μM) in the same incubation time. \$ $p < 0.05$, \$\$ $p < 0.01$, and \$\$\$\$ $p < 0.0001$ comparing to AuNPs at 400 μM in the same incubation time. Data are presented as mean value ± SD, $n = 1$.

Statistically significant reductions in cell viability of 19%, 28%, and 44% were observed after a 24-h incubation time with HAOA-AuNPs at 50, 200, and 400 μM, respectively, when compared to control ($p < 0.0001$). After a 48-h incubation time, these losses were: 13%, 19%, and 26%, respectively ($p \leq 0.0001$). HAOA-AuNPs induced toxicity in a dose-dependent manner; however,

increasing incubation time did not lead to greater toxicity. Indeed, a significant increase ($p < 0.0001$) of ~18% in cell viability was observed after a 48-h incubation time with HAOA-AuNPs at 400 μM when compared to the lower incubation time. Speculations can be made about the proliferative effect that the high local concentration of HA may be inducing on BxPC-3 cells over time. This effect was already demonstrated by others on human tendon derived cells [67].

For BBN-AuNPs, statistically significant decrease in cell viability of 9 and 27% were obtained after a 24-h incubation time with 200 and 400 μM of these AuNPs, respectively, when compared to control ($p = 0.007$; $p < 0.0001$). After a 48-h incubation time, cell viability losses were observed for all concentrations tested: 44%, 48%, and 52%, for 50, 200, and 400 μM of these AuNPs, respectively ($p < 0.0001$). BBN-AuNPs induced toxicity in a dose- and time- dependent manner. The presence of aggregates may be in the origin of the high cytotoxic effect observed for the 48-h incubation time even at lower concentrations.

A concentration in gold is considered to be cytotoxic when cell viability lower than 80 – 90% is obtained. Thus, after a 24-h incubation period, only HAOA-AuNPs at 50 μM and BBN-AuNPs at 50 μM or 200 μM were considered as non-toxic for the cells: cell viabilities of approximately 81%, 93% and 91%, respectively, were obtained. However, for the assays in which the presence of AuNPs during RT was assessed, it was decided to test HAOA-AuNPs at all concentrations. In these assays, cells are incubated with AuNPs for only 4 h. After that time, complete medium is changed and only internalized AuNPs remain within the cells. Because of that, it was speculated that a 4-h incubation time with HAOA-AuNPs at any of these concentrations would not reflect a cytotoxic effect on BxPC-3 cells. This 4-h incubation time was defined to be the optimal time for HAOA-AuNPs internalization in melanoma cells [62,68].

3.6. Impact of HAOA-AuNPs during RT

The potential of concomitant RT with HAOA-AuNPs in BxPC-3 cells was evaluated by MTT assay 48 and 72 h post-irradiation (Figure 3.6 and Figure 3.7) – to reinforce the previously selected 72-h incubation time as the optimal choice, it was decided to retest the cell viability results 48 and 72 h after irradiation. Cell viability was assessed for HAOA-AuNPs at 50, 200, and 400 μM and radiation doses ranging from 2 to 5 Gy.

For the 48-h post-irradiation time, the effect of the combined treatment for HAOA-AuNPs at 400 μM was not significantly different ($p > 0.3$) from the cells incubated with AuNPs alone. Thus, for this post-irradiation time, the loss in cell viability observed for the combined treatment seems to be only caused by HAOA-AuNPs, independently of the radiation dose. This may probably be due to the high cytotoxicity induced by AuNPs at this concentration. For that reason, the statistical results for the combined treatment are not presented here.

Neither 50 μM of HAOA-AuNPs alone neither 2 Gy alone induced a significant difference in cell viability when compared to the control ($p = 0.055$; $p = 0.12$). Nevertheless, the combined treatment induced a loss in cell viability of 21.6% ($p < 0.0001$). This effect was also observed for HAOA-AuNPs at 200 μM, where the combined treatment induced a loss in cell viability of approximately 30% ($p < 0.0001$). The effects of the combined treatment observed at 2 Gy for both AuNPs concentrations were not enhanced after irradiation with 3.5 and 5 Gy.

As previously observed (*see* subsection *3*.4), the effects caused by RT alone seem to be negligible at short incubation times probably due to the lag period as already discussed. Thus, it is important to use longer post-radiation incubation times to assess cell viability more accurately with MTT assay.

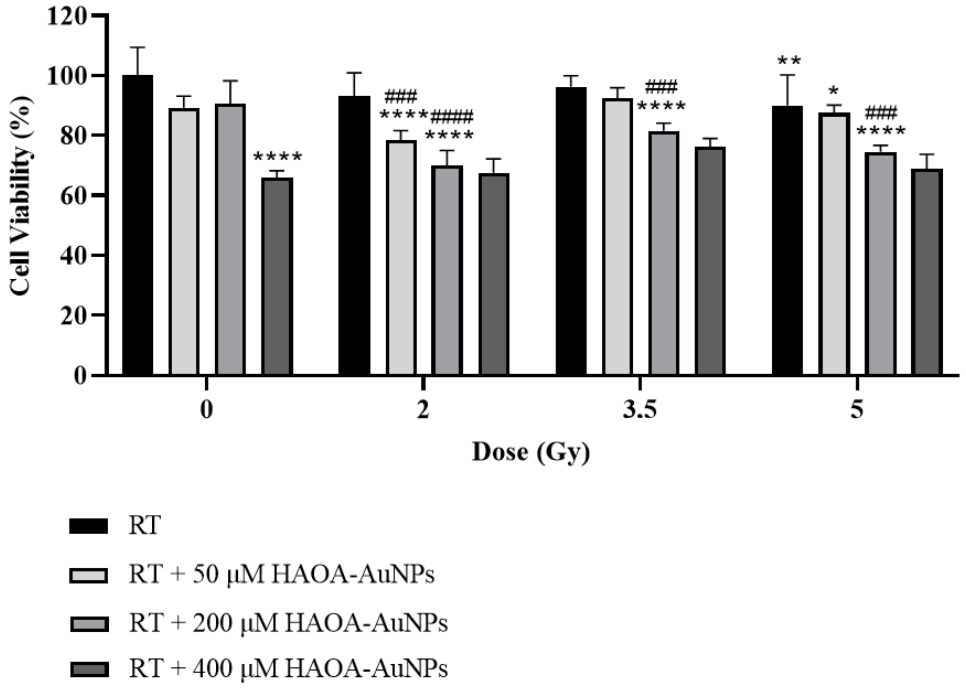

Figure 3.6 - Cell viability (%) of BxPC-3 cell line 48 h after irradiation with HAOA-AuNPs at different concentrations. *p < 0.05, **p < 0.01 and **** p < 0.0001 comparing to control. ### p < 0.001 and #### p < 0.0001 comparing to RT alone at the same radiation dose. Data are presented as mean value ± SD, $n = 1$.

The results of MTT assays performed 72 h post-irradiation are shown in Figure 3.7. No significant difference was obtained between 50 µM alone and the control ($p = 0.26$). On the other hand, a statistically significant difference in cell viability of approximately 20% and 35% for AuNPs alone at 200 and 400 µM, respectively, was obtained compared to the control ($p < 0.0001$).

Cell viability obtained for RT plus HAOA-AuNPs at 50 µM was not significantly different from RT alone for each radiation dose ($p > 0.6$). On the other hand, the combined treatment of RT with HAOA-AuNPs at 200 µM induced a mean loss in cell viability of approximately 40% when compared to control ($p < 0.0001$). Similarly, a statistically significant loss in cell viability was obtained when combining a radiation dose of 5 Gy with HAOA-AuNPs at 400 µM ($p < 0.0001$). For both situations, the effects caused by the combined treatment seem to be caused by an additive behaviour between RT and AuNPs.

Again, the effects of the combined treatment observed at 2 Gy for HAOA-AuNPs at 200 µM were not enhanced after irradiation with 3.5 and 5 Gy. This observation may be explained by the dose-dependent lag period, already explored before. In the presence of AuNPs during RT, the lag period could be even more accentuated since there could be more DNA damage to be repaired.

Discrepancies between results obtained with MTT and clonogenic assays have been reported. Authors that assessed the effect of RT with AuNPs through both assays have obtained lower gains with MTT assay than with clonogenic assays (this has already been discussed in section 1.5). Roa *et al.* performed irradiation with a ^{137}C source (γ-rays) at 2 Gy plus AuNPs of human prostate cancer cells (DU-145). At 24 h, AuNPs+RT led to an inhibition rate of 26.8% in cells proliferation, while clonogenic assay (performed 14 days after irradiation) led to a decrease in surviving fraction of 63.2% [69].

MTT assay evaluates the presence of cells which are alive through their metabolic activity. However, due to incapacity of cells to repair damage, part of them has poor or no cell proliferation ability and will eventually die. By its turn, clonogenic assays quantify as surviving cells those that have proliferation capacity, and thus can form colonies with more than 50 cells [58]. Therefore, the results obtained in this study may underestimate the true outcome of the combined treatment. In the future, clonogenic assays should also be performed aiming to corroborate the findings obtained from the MTT assay.

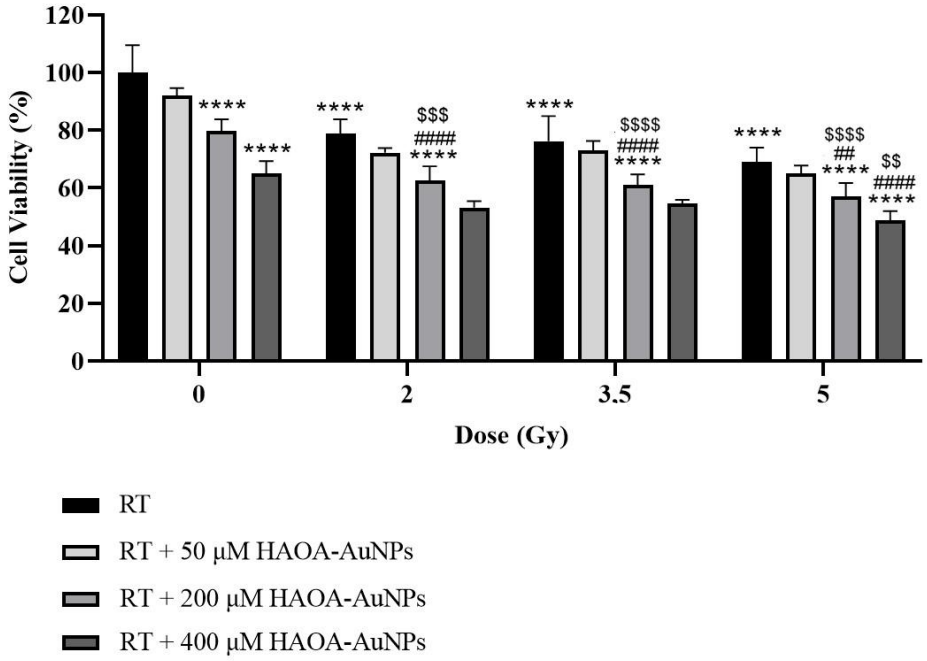

Figure 3.7 - Cell viability (%) of BxPC-3 cell line 72 h after irradiation with HAOA-AuNPs at different concentrations. **** $p < 0.0001$ comparing to control. ## $p < 0.01$ and #### $p < 0.0001$ comparing to RT alone at the same radiation dose. $$ $p < 0.01$, $$$ $p < 0.001$ and $$$$ $p < 0.0001$ comparing to HAOA-AuNPs at the same concentration in the absence of RT. Data are presented as mean value ± SD, $n = 1$.

3.7. Impact of size and coating: BBN-AuNPs during RT

The potential of concomitant RT with BBN-AuNPs in BxPC-3 cells was evaluated by MTT assay 48 and 72 h post-irradiation. Cell viability was assessed for BBN-AuNPs at 50 and 200 μM and radiation doses ranging from 2 to 5 Gy. Results are presented in Figure 3.8.

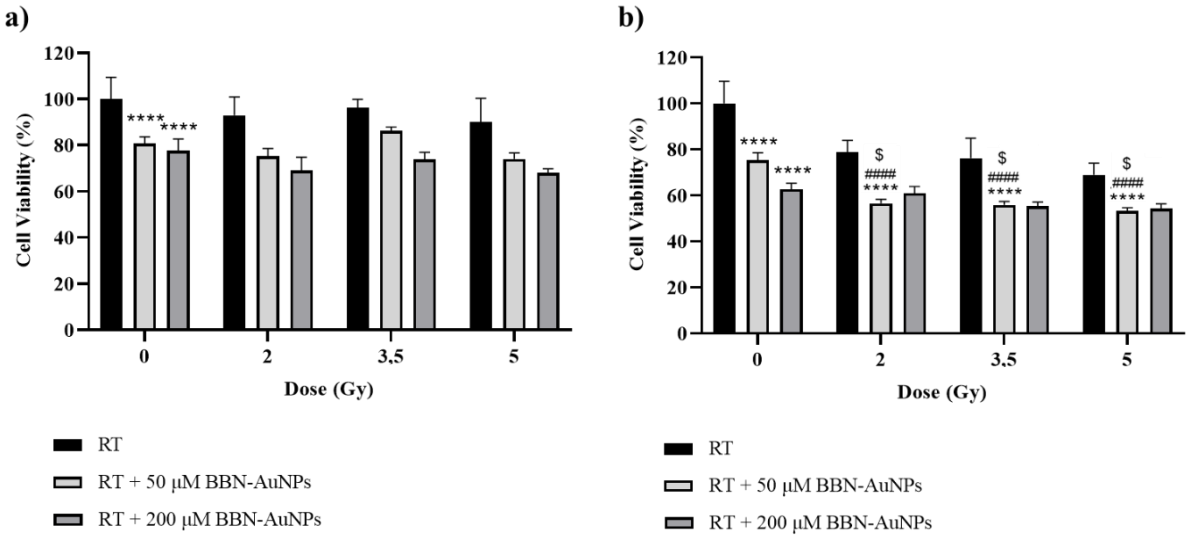

Figure 3.8 - Cell viability (%) of BxPC-3 cell line (a) 48 h and (b) 72 h after irradiation with 50 and 200 μM of BBN-AuNPs. **** $p < 0.0001$ comparing to control. #### $p < 0.0001$ comparing to RT alone at the same radiation dose. $ $p < 0.05$ comparing to BBN-AuNPs at the same concentration in the absence of radiation. Data are presented as mean value ± SD, n = 1.

For the 48-h post irradiation time, the effect of the combined treatment for BBN-AuNPs at 50 and 200 μM was not significantly different from the group of cells incubated with these AuNPs alone ($p > 0.4$). This was also observed for the combined treatment for BBN-AuNPs at 200 μM, 72-h post-irradiation ($p > 0.3$). In these situations, the loss in cell viability observed for the combined treatment at all radiation doses seems to be only caused by BBN-AuNPs.

For the 72-h post-irradiation time, the combined treatment of RT with BBN-AuNPs at 50 μM induced a mean loss in cell viability of approximately 45% when compared to control ($p < 0.0001$). Moreover, the effects caused by the combined treatment seem to be caused by an additive behaviour. A similar result was obtained for the combined treatment with HAOA-AuNPs at 200 μM, for the same post-irradiation time (*see* subsection 3.6). As the combined treatment using BBN-AuNPs at a low concentration led to a similar loss of viability compared to the combined treatment using HAOA-AuNPs at a higher concentration, there seems to be an influence of the size and/or coating of AuNPs on the effect of RT. However, as the average particle size obtained for BBN-AuNPs was not concordant between DLS and AFM (*see* subsection 3.1), it is not possible to draw a precise conclusion about the influence of the size on the combined treatment of RT plus AuNPs.

3.8. Impact of field size during RT with AuNPs

The potential of HAOA-AuNPs during irradiation of BxPC-3 cells with different field sizes was evaluated by MTT assay 72 h post-irradiation. Cell viability was assessed for HAOA-AuNPs at 50, 100, and 200 µM, and 2 Gy of radiation dose delivered with field sizes of 8x8, 20x20, and 30x30 cm^2. A dosimetric analysis to assess the dose distribution within 8x8 and 30x30 cm^2 field sizes was performed (*see* Appendix). For the 8x8 cm^2 field size, the planned mean dose was 1.983 ± 0.017 Gy. For the 30x30 cm^2 field size, the planned mean dose was 2.014 ± 0.004 Gy. Cell viability results are presented in Figure 3.9.

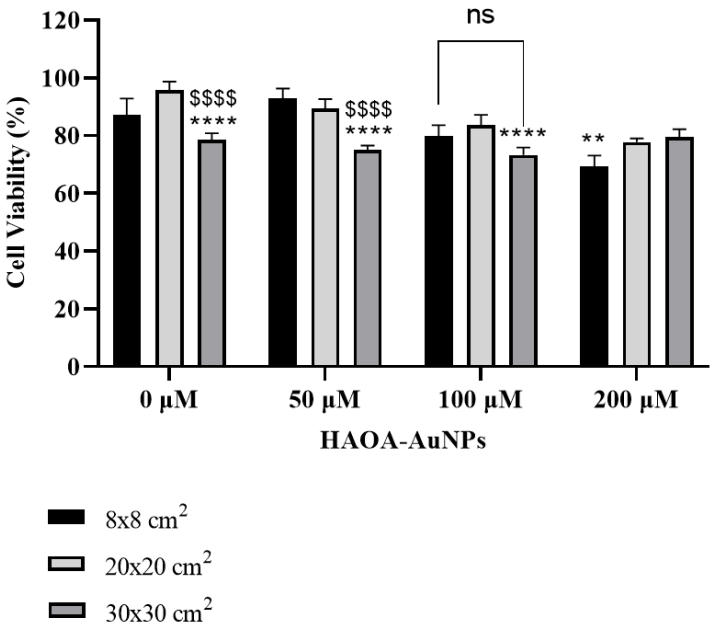

Figure 3.9 - Cell viability (%) of BxPC-3 cell line 72 h after irradiation with 2 Gy and HAOA-AuNPs at 50, 100, and 200 µM. Field sizes of 8x8, 20x20, and 30x30 cm^2 were used during irradiation. ** $p < 0.01$ and **** $p < 0.0001$ comparing to irradiation with 20x20 cm^2 field size at the same concentration of HAOA-AuNPs. $$$$ $p < 0.0001$ comparing to irradiation with 8x8 cm^2 field size at the same concentrations of HAOA-AuNPs. ns = not significant. Data are presented as mean value ± SD, $n = 1$.

With increasing field size, it was expected that the effects caused by RT could be accentuated in the presence of AuNPs. Thus, for combined treatment, greater cell viability loss was expected with increasing field size. The increase in the number of low-energy scattered photons produced in the phantom with increasing the field size, leads to an increase in local dose deposition if high-Z materials are present in the medium (there is a higher probability of occurring photoelectric effect). However, in the presence of HAOA-AuNPs, this was only observed for AuNPs at 50 µM. Thus, these results remain inconclusive and should be re-tested in the future.

For RT alone, the dose delivered to the cells is independent of the beam spectrum. However, for cells without HAOA-AuNPs, a remarkable decrease in cell viability using a 30x30 cm^2 field size was obtained when compared with both 8x8 and 20x20 cm^2 field sizes ($p < 0.0001$). As this was not expected to happen, the need to repeat this assay is once again emphasised.

3.9. Impact of free-flattening filter beam during RT with AuNPs

The potential of HAOA-AuNPs during irradiation with a FFF beam of BxPC-3 cells was evaluated by MTT assay 72 h post-irradiation. Cell viability was assessed for HAOA-AuNPs at 200 μM and 2 Gy of radiation dose. Because with FFF a configuration, the beam intensity is not uniform (i.e., the dose distribution is not homogenous), a dosimetric analysis was performed to group the cells according to the planned radiation dose (*see* Appendix). Two groups of wells (from the same 96-well plate) receiving a similar radiation dose – with a maximum difference of 3% between each group – were created. Group 1 was composed by the wells that were irradiated with a planned mean dose of 2,112 ± 0.017 Gy while Group 2 was composed by wells that were irradiated with a planned mean dose of 2,164 Gy ± 0.017 Gy. Cell viability results for both groups are presented in Figure 3.10.

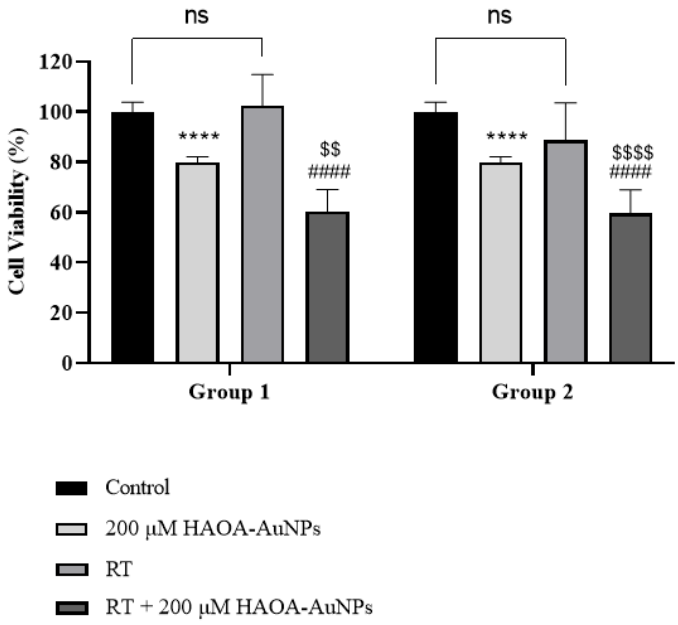

Figure 3.10 - Cell viability (%) of BxPC-3 cell line 72 h after irradiation with 2 Gy in a FFF configuration and 200 μM of HAOA-AuNPs. Group 1 represent cells receiving a planned mean dose of 2.11 Gy, and Group 2 represent cells receiving a planned mean dose of 2.16 Gy. **** $p < 0.0001$ comparing to control. #### $p < 0.0001$ comparing to RT alone at the same group. $$ $p < 0.01$ and $$$$ $p < 0.0001$ comparing to HAOA-AuNPs alone at the same group. Data are presented as mean value ± SD, $n = 1$.

For 200 μM of HAOA-AuNPs plus RT, a remarkable decrease in cell viability when comparing to control was obtained: a mean of approximately 40% for both groups ($p < 0.0001$). For RT delivered with a FFF beam, it was expected that the effects caused by RT would be accentuated in the presence of AuNPs because of the higher proportion of low-energy photons in the primary path. Thus, the combined treatment was expected to induce greater cell viability losses compared to RT delivered with a flattening filter (FF) beam.

Although in this case the planned dose was slightly higher than 2 Gy (i.e., the planned dose of the standard plan), the results obtained with a FFF beam *versus* FF beam (standard plan) will be cautiously compared. Since on average the same loss in cell viability was obtained for RT delivered

with a FF beam plus AuNPs (*see* Figure 3.7), the use of the FFF beam does not seem to have led to a different impact on cell viability.

Unexpectedly, in this assay, RT alone did not produce statistically significant decrease in cell viability compared to the control ($p > 0.05$), for both group 1 and 2, contradicting previous results (*see* Figure 3.7). These opposing findings reveal the importance of re-testing the impact of FFF beam on the irradiation of BxPC-3 cells with HAOA-AuNPs in the future.

3.10. Dosimetry

In this study, most cells irradiation was performed with a uniform beam produced using a FF placed on the beam path through the standard plan configuration (Plan 1). For the field size of 20x20 cm^2, the dosimetric analysis for a planned dose of 2 Gy revealed a homogeneous dose distribution within the irradiated wells (Figure 3.11, a). After exclusion of wells from the periphery of the plate (process done for all assays), the planned dose to the wells of interest averaged 2.000 ± 0.004 Gy.

Two plans using multiple segments of different field sizes were tested to assess the possibility to irradiate the cell plates with various dose values in future experiments. To ensure a homogeneous dose distribution to a subset of wells, it will be necessary to discard some columns of wells. Considering the columns of wells that can be used (highlighted with colour in Figure 3.11), Plan 2, composed by two segments (Figure 3.11, b), allows irradiation with two averaged planned doses: 2.002 ± 0.041 Gy and 3.478 ± 0.028 Gy. Plan 3 allows irradiation with three averaged planned doses: 1.957 ± 0.031 Gy, 3.541 ± 0.041 Gy, and 5.011 ± 0.021 Gy (Figure 3.11,c).

For all the three plans, a relative difference (%) in the planned dose to the wells ≤ 4% was obtained compared to the planned dose of the reference well. The dose profile of the planned doses was also traced for all the three Plans and is shown in Figure 3.11, d.

This analysis is based on the planned dose distribution obtained by the treatment planning systems whose dose calculation algorithms have its own dosimetric accuracy and limitations, especially in the presence of large heterogeneities. Although the dose calculated was based on the planning CT of the phantom used for irradiation, the presence of air cavities between the PMMA phantom plates and within the wells of the cell plates may result in differences between the planned and delivered dose in the cells.

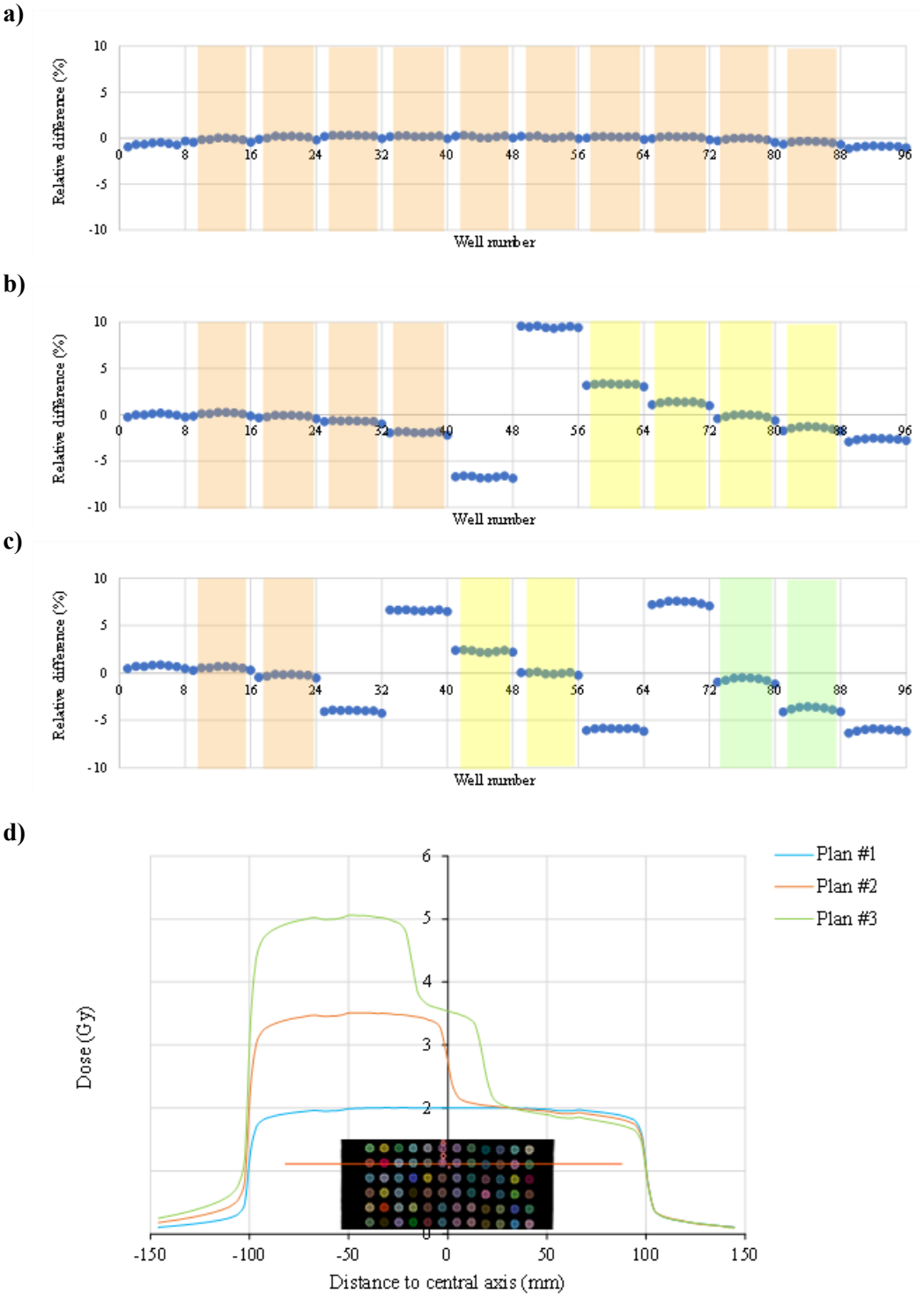

Figure 3.11 – Relative difference (%) between the planned dose in the reference well, and the planned dose to every well of the plate for (a) Plan 1, (b) Plan 2, and (c) Plan 3. Coloured regions represent regions of greater dose homogeneity. Wells within these regions are the wells of interest. (d) Dose profile along a 96-well plate column (represented crossed by a red line) for the three different plans.

4. Conclusion and Future Perspectives

The present master dissertation consisted of an exploratory analysis of the potential of AuNPs of different sizes and coatings, HAOA-AuNPs and BBN-AuNPs, on human pancreatic adenocarcinoma BxPC-3 cells irradiated with a 6 MV photon beam. Cytotoxicity assays revealed that incubation of BxPC-3 cells with 50, 200, and 400 μM of HAOA-AuNPs and BBN-AuNPs for 24 and 48 h represented cytotoxicity in a dose-dependent manner. In addition, BBN-AuNPs also showed toxicity in a time-dependent manner.

Cell viability assays performed 48 h post-irradiation showed that the effect of RT alone on BxPC-3 cells seem to be negligible for short post-irradiation incubation times. This is probably due to the lag period of these cells after RT. The 72-h incubation time proved to be more adequate because it translated more reliably cell viability values after irradiation. Thus, to assess cell viability more accurately with MTT assay, it is important to use long post-radiation incubation times.

For the 72-h post-irradiation time, the combined treatment of RT either with HAOA-AuNPs at 200 μM, or with BBN-AuNPs at 50 μM, led to a mean cell viability loss of 40 and 45%, respectively, compared to no treatment. In addition, the effect of the combined treatment seems to have origin from an additive behaviour caused by RT and AuNPs. Thus, there appears to be a potential benefit from the combined treatment for both formulations of AuNPs. Moreover, the impact of the beam spectrum on the potential of the combined treatment did not produce differences in cell viability loss compared to the standard setup. However, this result should be re-tested.

Because this was an exploratory study, all assays were performed with only one replicate. A higher number of experiments should be performed in the future to corroborate the results obtained here. Additionally, clonogenic assays should also be performed to more accurately evaluate the potential of concomitant RT with AuNPs.

The irradiation of BxPC-3 cells was performed after a 4-h incubation with HAOA-AuNPs and BBN-AuNPs based on others' findings. However, the optimal internalization time is cell-line dependent. In this work, it was assumed that a 4-h incubation was sufficient to allow an effective internalization of AuNPs into cells. It is also important to note that, besides size, BBN-AuNPs and HAOA-AuNPs also present with different coating. As mentioned before, coating may interfere with the level of cellular internalization, cytotoxicity, stability, among other factors. Consequently, it may also play a key role in the potential of the combined treatment of RT with AuNPs. A comparison between AuNPs where there was only one studied variable would be more rigorous; for instance, to test HAOA-AuNPs and BBN-AuNPs with the same size.

In the future, it would also be interesting to investigate the cytotoxicity of AuNPs in a lower concentration range, since the concentrations of AuNPs tested here induced relevant losses in cell viability on their own. This may be related to the fact that only an additive behaviour seems to be present for the combined treatment. It would also be interesting to assess whether a higher level of cytotoxicity is related to a higher cellular uptake of AuNPs by BxPC-3 cells. In addition, the evaluation of AuNPs cytotoxicity in a non-tumour human cell line would provide important data on the safety of HAOA-AuNPs and BBN-AuNPs for healthy tissues.

It would be of great value to conduct future tests to evaluate the possible chemical and/or biological bases of the potential success of the combined treatment. An evaluation of BxPC-3 cells irradiated with and without AuNPs based on the γH2AX *foci*; the level of ROS; cell distribution along the cell cycle phases; and levels of cell apoptosis, would be very interesting to perform. To explore the potential of HAOA-AuNPs and BBN-AuNPs in other human pancreatic tumour cells, PANC-1 and MIA PaCa-2 cell lines could also be tested.

Finally, *in vivo* studies would be important to evaluate the biodistribution, biocompatibility and clearance of both HAOA-AuNPs and BBN-AuNPs. The SBRT technique is based on delivering ablative RT doses in a short number of fractions. If AuNPs were guaranteed to be present in the tumour cells during the SBRT treatment time, the local effects of the combined treatment would always be guaranteed, and constant administration of AuNPs would be avoided. It is also necessary to study in depth all the characteristics of AuNPs that may influence their potential during RT in order to assess which features exponentiates the effects of the combined treatment. It is important to define the most adequate size, coating, functionalization, concentration, optimal regime of administration, optimal beam, among many other factors. Although the road to clinical trials for AuNPs is still long, one thing seems certain – AuNPs appear to bring some hope to the treatment of pancreatic cancer with RT.

5. References

[1] F. Campbell and C. S. Verbeke, *Pathology of the Pancreas*, 1st ed. London: Springer, 2013.

[2] World Health Organization, "Pancreatic Cancer Fact Sheet," *International Agency for Research on Cancer*, 2020. https://gco.iarc.fr/today/fact-sheets-cancers (accessed Nov. 08, 2021).

[3] A. Rebelo and C. Reis, "Emerging therapeutic nanotechnologies in pancreatic cancer: advances, risks and challenges," *Ther Deliv*, vol. 9, no. 10, pp. 691–694, Oct. 2018, doi: 10.4155/TDE-2018-0048.

[4] M. Beyzadeoglu, G. Ozyigit, and C. Ebruli, *Basic Radiation Oncology*, 1st ed. Berlin, Heidelberg: Springer, 2010. doi: 10.1007/978-3-642-11666-7.

[5] A. McGuigan, P. Kelly, R. C. Turkington, C. Jones, H. G. Coleman, and R. S. McCain, "Pancreatic cancer: A review of clinical diagnosis, epidemiology, treatment and outcomes," *World J Gastroenterol*, vol. 24, no. 43, pp. 4846–4861, Nov. 2018, doi: 10.3748/wjg.v24.i43.4846.

[6] P. Rawla, T. Sunkara, and V. Gaduputi, "Epidemiology of Pancreatic Cancer: Global Trends, Etiology and Risk Factors," *World J Oncol*, vol. 10, no. 1, pp. 10–27, 2019, doi: 10.14740/wjon1166.

[7] F. M. Khan, J. P. Gibbons, and P. W. Sperduto, *Khan's Treatment Planning in Radiation Oncology*, 4th ed. Philadelphia: Wolters Kluwer, 2016.

[8] J. Werner, S. E. Combs, C. Springfeld, W. Hartwig, T. Hackert, and M. W. Büchler, "Advanced-stage pancreatic cancer: Therapy options," *Nat Rev Clin Oncol*, vol. 10, pp. 323–333, Jun. 2013, doi: 10.1038/nrclinonc.2013.66.

[9] W. Park, A. Chawla, and E. M. O'Reilly, "Pancreatic Cancer: A Review," *JAMA - Journal of the American Medical Association*, vol. 326, no. 9, pp. 851–862, Sep. 2021, doi: 10.1001/jama.2021.13027.

[10] E. Landau and S. Kalnicki, "The Evolving Role of Radiation in Pancreatic Cancer," *Surgical Clinics of North America*, vol. 98, no. 1, pp. 113–125, Feb. 2018, doi: 10.1016/j.suc.2017.09.008.

[11] A. L. Coveler, J. M. Herman, D. M. Simeone, and E. G. Chiorean, “Localized pancreatic cancer: multidisciplinary management,” *Am Soc Clin Oncol Educ Book*, vol. 35, no. 36, pp. e217–e226, May 2016, doi: 10.1200/EDBK_160827.

[12] M. I. Bittner, A. L. Grosu, and T. B. Brunner, “Comparison of toxicity after IMRT and 3D-conformal radiotherapy for patients with pancreatic cancer - A systematic review,” *Radiotherapy and Oncology*, vol. 114, no. 1, pp. 117–121, Jan. 2015, doi: 10.1016/j.radonc.2014.11.043.

[13] A. R. P. de Sousa, “Análise de eficácia e custo-efetividade de diferentes tratamentos do cancro do pâncreas localmente avançado,” Escola Superior de Saúde do Instituto Politécnico do Porto, 2020.

[14] Z. Kuncic and S. Lacombe, “Nanoparticle radio-enhancement: Principles, progress and application to cancer treatment,” *Phys Med Biol*, vol. 63, no. 2, Jan. 2018, doi: 10.1088/1361-6560/aa99ce.

[15] S. Her, D. A. Jaffray, and C. Allen, “Gold nanoparticles for applications in cancer radiotherapy: Mechanisms and recent advancements,” *Adv Drug Deliv Rev*, vol. 109, pp. 84–101, Jan. 2017, doi: 10.1016/j.addr.2015.12.012.

[16] K. Bromma and D. B. Chithrani, “Advances in gold nanoparticle-based combined cancer therapy,” *Nanomaterials*, vol. 10, no. 9, pp. 1–25, Aug. 2020, doi: 10.3390/nano10091671.

[17] J. Schuemann *et al.*, “Roadmap to clinical use of gold nanoparticles for radiation sensitization,” *Int J Radiat Oncol Biol Phys*, vol. 94, no. 1, pp. 189–205, Jan. 2016, doi: 10.1016/j.ijrobp.2015.09.032.

[18] S. Martelli and J. C. L. Chow, “Dose enhancement for the flattening-filter-free and flattening-filter photon beams in nanoparticle-enhanced radiotherapy: A monte carlo phantom study,” *Nanomaterials*, vol. 10, no. 4, Apr. 2020, doi: 10.3390/nano10040637.

[19] R. I. Berbeco *et al.*, “DNA damage enhancement from gold nanoparticles for clinical MV photon beams,” *Radiat Res*, vol. 178, no. 6, pp. 604–608, Dec. 2012, doi: 10.1667/RR3001.1.

[20] A. Detappe, P. Tsiamas, W. Ngwa, P. Zygmanski, M. Makrigiorgos, and R. Berbeco, “The effect of flattening filter free delivery on endothelial dose enhancement with gold nanoparticles,” *Med Phys*, vol. 40, no. 3, 2013, doi: 10.1118/1.4791671.

[21] M. C. Bonferoni *et al.*, “Electrochemotherapy of deep-seated tumors: State of art and perspectives as possible ‘epr effect enhancer’ to improve cancer nanomedicine efficacy,” *Cancers (Basel)*, vol. 13, no. 17, p. 4437, Sep. 2021, doi: 10.3390/cancers13174437.

[22] C. O. Silva *et al.*, “Bioproduction of gold nanoparticles for photothermal therapy,” *Ther Deliv*, vol. 7, no. 5, pp. 287–304, May 2016, doi: 10.4155/tde-2015-0011.

[23] M. Amaral *et al.*, “Gold-based nanoplataform for the treatment of anaplastic thyroid carcinoma: A step forward,” *Cancers (Basel)*, vol. 13, no. 6, pp. 1–24, Mar. 2021, doi: 10.3390/cancers13061242.

[24] Y. Sakurai and H. Harashima, “Hyaluronan-modified nanoparticles for tumor-targeting,” *Expert Opin Drug Deliv*, vol. 16, no. 9, pp. 915–936, Sep. 2019, doi: 10.1080/17425247.2019.1645115.

[25] H. J. Wei, T. Yin, Z. Zhu, P. F. Shi, Y. Tian, and C. Y. Wang, “Expression of CD44, CD24 and ESA in pancreatic adenocarcinoma cell lines varies with local microenvironment,” *Hepatobiliary and Pancreatic Diseases International*, vol. 10, no. 4, pp. 428–434, 2011, doi: 10.1016/S1499-3872(11)60073-8.

[26] M. Kus-liśkiewicz, P. Fickers, and I. ben Tahar, “Biocompatibility and cytotoxicity of gold nanoparticles: Recent advances in methodologies and regulations,” *Int J Mol Sci*, vol. 22, no. 20, Oct. 2021, doi: 10.3390/ijms222010952.

[27] A. Ku, V. J. Facca, Z. Cai, and R. M. Reilly, “Auger electrons for cancer therapy – a review,” *EJNMMI Radiopharm Chem*, vol. 4, no. 1, pp. 1–36, Oct. 2019, doi: 10.1186/s41181-019-0075-2.

[28] J. H. Hubbell and S. M. Seltzer, “Tables of X-Ray Mass Attenuation Coefficients and Mass Energy-Absorption Coefficients (version 1.4),” 2004. http://physics.nist.gov/xaamdi (accessed Aug. 05, 2022).

[29] R. A. Powsner and E. R. Powsner, *Essential Nuclear Medicine Physics*, 2nd ed. Oxford: Blackwell Publishing, 2008. doi: 10.1002/9780470752890.

[30] A. van der Kogel and M. Joiner, *Basic Clinical Radiobiology*, 4th ed. Great Britain: Hodder Arnold, 2009.

[31] Y. Chen, J. Yang, S. Fu, and J. Wu, “Gold nanoparticles as radiosensitizers in cancer radiotherapy,” *Int J Nanomedicine*, vol. 15, pp. 9407–9430, 2020, doi: 10.2147/IJN.S272902.

[32] Y. Pan, M. Bartneck, and W. Jahnen-Dechent, “Cytotoxicity of gold nanoparticles,” in *Methods in Enzymology*, vol. 509, Elsevier Inc., 2012, pp. 225–242. doi: 10.1016/B978-0-12-391858-1.00012-5.

[33] D. Mateo, P. Morales, A. Ávalos, and A. I. Haza, “Oxidative stress contributes to gold nanoparticle-induced cytotoxicity in human tumor cells,” *Toxicol Mech Methods*, vol. 24, no. 3, pp. 161–172, Mar. 2014, doi: 10.3109/15376516.2013.869783.

[34] M. Bhamidipati and L. Fabris, “Multiparametric assessment of gold nanoparticle cytotoxicity in cancerous and healthy cells: the role of size, shape, and surface chemistry,” *Bioconjug Chem*, vol. 28, no. 2, pp. 449–460, Feb. 2017, doi: 10.1021/acs.bioconjchem.6b00605.

[35] A. Woźniak *et al.*, “Size and shape-dependent cytotoxicity profile of gold nanoparticles for biomedical applications,” *J Mater Sci Mater Med*, vol. 28, no. 6, Jun. 2017, doi: 10.1007/s10856-017-5902-y.

[36] N. Chen, W. Yang, Y. Bao, H. Xu, S. Qin, and Y. Tu, “BSA capped Au nanoparticle as an efficient sensitizer for glioblastoma tumor radiation therapy,” *RSC Adv*, vol. 5, pp. 40514–40520, 2015, doi: 10.1039/c5ra04013b.

[37] Y. Liu *et al.*, “The dependence of radiation enhancement effect on the concentration of gold nanoparticles exposed to low- and high-LET radiations,” *Physica Medica*, vol. 31, no. 3, pp. 210–218, May 2015, doi: 10.1016/j.ejmp.2015.01.006.

[38] H. Hau *et al.*, “Dose enhancement and cytotoxicity of gold nanoparticles in colon cancer cells when irradiated with kilo- and mega-voltage radiation,” *Bioeng Transl Med*, vol. 1, no. 1, pp. 94–102, Mar. 2016, doi: 10.1002/btm2.10007.

[39] S. Soleymanifard, A. Rostami, S. A. Aledavood, M. M. Matin, and A. Sazgarnia, “Increased radiotoxicity in two cancerous cell lines irradiated by low and high energy photons in the presence of thio-glucose bound gold nanoparticles,” *Int J Radiat Biol*, vol. 93, no. 4, pp. 407–415, Apr. 2017, doi: 10.1080/09553002.2017.1268282.

[40] S. Özçelik, and G. Pratx, “Nuclear-targeted gold nanoparticles enhance cancer cell radiosensitization,” *Nanotechnology*, vol. 31, no. 41, p. 8, 2020, doi: 10.1088/1361-6528/aba02b.

[41] A. Tudda *et al.*, “Breast radiotherapy with kilovoltage photons and gold nanoparticles as radiosensitizer: An in vitro study,” *Med Phys*, vol. 49, no. 1, pp. 568–578, Jan. 2022, doi: 10.1002/mp.15348.

[42] A. Subiel, R. Ashmore, and G. Schettino, “Standards and methodologies for characterizing radiobiological impact of high-Z nanoparticles,” *Theranostics*, vol. 6, no. 10, pp. 1651–1671, 2016, doi: 10.7150/thno.15019.

[43] C. Wang, Y. Jiang, X. Li, and L. Hu, “Thioglucose-bound gold nanoparticles increase the radiosensitivity of a triple-negative breast cancer cell line (MDA-MB-231),” *Breast Cancer*, vol. 22, no. 4, pp. 413–420, Jul. 2015, doi: 10.1007/s12282-013-0496-9.

[44] T. Wolfe *et al.*, “Targeted gold nanoparticles enhance sensitization of prostate tumors to megavoltage radiation therapy in vivo,” *Nanomedicine*, vol. 11, no. 5, pp. 1277–1283, Jul. 2015, doi: 10.1016/j.nano.2014.12.016.

[45] P. Liu *et al.*, “Silver nanoparticles outperform gold nanoparticles in radiosensitizing U251 cells in vitro and in an intracranial mouse model of glioma,” *Int J Nanomedicine*, vol. 11, pp. 5003–5014, Oct. 2016, doi: 10.2147/IJN.S115473.

[46] A. Saberi, D. Shahbazi-Gahrouei, M. Abbasian, M. Fesharaki, A. Baharlouei, and Z. Arab-Bafrani, “Gold nanoparticles in combination with megavoltage radiation energy increased radiosensitization and apoptosis in colon cancer HT-29 cells,” *Int J Radiat Biol*, vol. 93, no. 3, pp. 315–323, Mar. 2017, doi: 10.1080/09553002.2017.1242816.

[47] X. Zhang, H. Wang, J. A. Coulter, and R. Yang, “Octaarginine-modified gold nanoparticles enhance the radiosensitivity of human colorectal cancer cell line LS180 to megavoltage radiation,” *Int J Nanomedicine*, vol. 13, pp. 3541–3552, Jun. 2018, doi: 10.2147/IJN.S161157.

[48] F. Kazmi, K. A. Vallis, B. A. Vellayappan, A. Bandla, D. Yukun, and R. Carlisle, “Megavoltage radiosensitization of gold nanoparticles on a glioblastoma cancer cell line using a clinical platform,” *Int J Mol Sci*, vol. 21, no. 2, Jan. 2020, doi: 10.3390/ijms21020429.

[49] F. Brero *et al.*, “Hadron therapy, magnetic nanoparticles and hyperthermia: A promising combined tool for pancreatic cancer treatment,” *Nanomaterials*, vol. 10, no. 10, pp. 1–17, Oct. 2020, doi: 10.3390/nano10101919.

[50] A. Detappe *et al.*, “Advanced multimodal nanoparticles delay tumor progression with clinical radiation therapy,” *Journal of Controlled Release*, vol. 238, pp. 103–113, Sep. 2016, doi: 10.1016/j.jconrel.2016.07.021.

[51] A. Yoshida *et al.*, “Gold nanoparticle-incorporated molecularly imprinted microgels as radiation sensitizers in pancreatic cancer,” *ACS Appl Bio Mater*, vol. 2, no. 3, pp. 1177–1183, Mar. 2019, doi: 10.1021/acsabm.8b00766.

[52] Z. Wang *et al.*, “The PPARγ agonist rosiglitazone enhances the radiosensitivity of human pancreatic cancer cells,” *Drug Des Devel Ther*, vol. 14, pp. 3099–3110, 2020, doi: 10.2147/DDDT.S242557.

[53] B. Tan, Y. Huang, B. Zhang, and N. Lin, “The effect of ibrutinib on radiosensitivity in pancreatic cancer cells by targeting EGFR/AKT/mTOR signaling pathway,” *Biomedicine and Pharmacotherapy*, vol. 128, Aug. 2020, doi: 10.1016/j.biopha.2020.110133.

[54] K. Schwarz, S. Dobiasch, L. Nguyen, D. Schilling, and S. E. Combs, “Modification of radiosensitivity by Curcumin in human pancreatic cancer cell lines,” *Sci Rep*, vol. 10, no. 1, Dec. 2020, doi: 10.1038/s41598-020-60765-1.

[55] Y. Xu *et al.*, “Disulfiram alone functions as a radiosensitizer for pancreatic cancer both in vitro and in vivo,” *Front Oncol*, vol. 11, Sep. 2021, doi: 10.3389/fonc.2021.683695.

[56] W. Waissi, J. C. Amé, C. Mura, G. Noël, and H. Burckel, “Gemcitabine-based chemoradiotherapy enhanced by a PARP inhibitor in pancreatic cancer cell lines,” *Int J Mol Sci*, vol. 22, no. 13, Jul. 2021, doi: 10.3390/ijms22136825.

[57] P. Price and T. J. McMillan, “Use of the tetrazolium assay in measuring the response of human tumor cells to ionizing radiation,” *Cancer Res*, vol. 50, no. 5, pp. 1392–1396, Mar. 1990.

[58] K. Buch, T. Peters, T. Nawroth, M. Sänger, H. Schmidberger, and P. Langguth, “Determination of cell survival after irradiation via clonogenic assay versus multiple MTT assay - a comparative study,” *Radiation Oncology*, vol. 7, no. 1, pp. 1–6, 2012, doi: 10.1186/1748-717X-7-1.

[59] E. Shahhoseini *et al.*, “Combined effects of gold nanoparticles and ionizing radiation on human prostate and lung cancer cell migration,” *Int J Mol Sci*, vol. 20, no. 18, p. 4488, Sep. 2019, doi: 10.3390/ijms20184488.

[60] X. Zhang *et al.*, “Enhanced radiation sensitivity in prostate cancer by gold-nanoparticles,” *Clinical and Investigative Medicine*, vol. 31, no. 3, pp. E160–E167, 2008, doi: 10.25011/cim.v31i3.3473.

[61] T. Kong *et al.*, “Enhancement of radiation cytotoxicity in breast-cancer cells by localized attachment of gold nanoparticles,” *Small*, vol. 4, no. 9, pp. 1537–1543, Sep. 2008, doi: 10.1002/smll.200700794.

[62] J. Lopes, J. M. P. Coelho, P. M. C. Vieira, A. S. Viana, M. M. Gaspar, and C. Reis, “Preliminary assays towards melanoma cells using phototherapy with gold-based nanomaterials,” *Nanomaterials*, vol. 10, no. 8, pp. 1–14, Aug. 2020, doi: 10.3390/nano10081536.

[63] F. Silva *et al.*, “Interrogating the role of receptor-mediated mechanisms: biological fate of peptide-functionalized radiolabeled gold nanoparticles in tumor mice,” *Bioconjug Chem*, vol. 27, no. 4, pp. 1153–1164, 2016, doi: 10.1021/acs.bioconjchem.6b00102.

[64] K. T. Jayaprakash *et al.*, “A high-throughput in vitro radiobiology platform for megavoltage photon linear accelerator studies,” *Applied Sciences (Switzerland)*, vol. 12, no. 3, 2022, doi: 10.3390/app12031456.

[65] N. Masoudi-Khoram *et al.*, “Differential miRNAs expression pattern of irradiated breast cancer cell lines is correlated with radiation sensitivity,” *Sci Rep*, vol. 10, no. 1, pp. 1–12, 2020, doi: 10.1038/s41598-020-65680-z.

[66] M. H. Tan *et al.*, “Characterization of a new primary human pancreatic tumor line,” *Cancer Invest*, vol. 4, no. 1, pp. 15–23, 1986, doi: 10.3109/07357908609039823.

[67] C. Berardi Anna, “Hyaluronic acid increases tendon derived cell viability and proliferation in vitro: comparative study of two different hyaluronic acid preparations by molecular weight,” *Muscles Ligaments Tendons J*, vol. 7, no. 2, p. 208, 2017, doi: 10.11138/mltj/2017.7.2.208.

[68] J. Lopes *et al.*, “Proof-of-concept study of multifunctional hybrid nanoparticle system combined with nir laser irradiation for the treatment of melanoma,” *Biomolecules*, vol. 11, no. 4, Apr. 2021, doi: 10.3390/biom11040511.

[69] W. Roa *et al.*, “Gold nanoparticle sensitize radiotherapy of prostate cancer cells by regulation of the cell cycle,” *Nanotechnology*, vol. 20, no. 37, 2009, doi: 10.1088/0957-4484/20/37/375101.

6. Appendix

A. Dosimetry analysis

a)

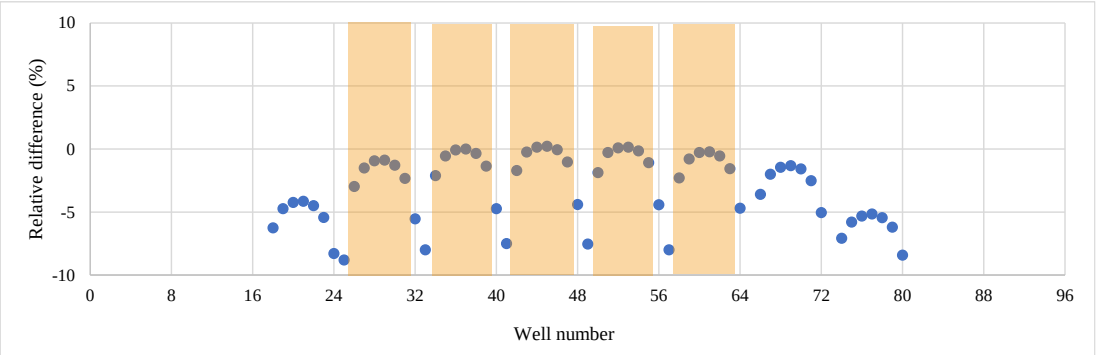

b)

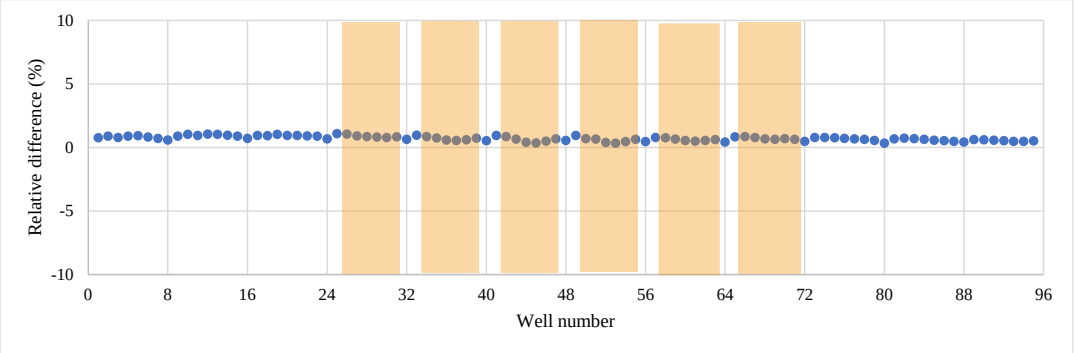

c)

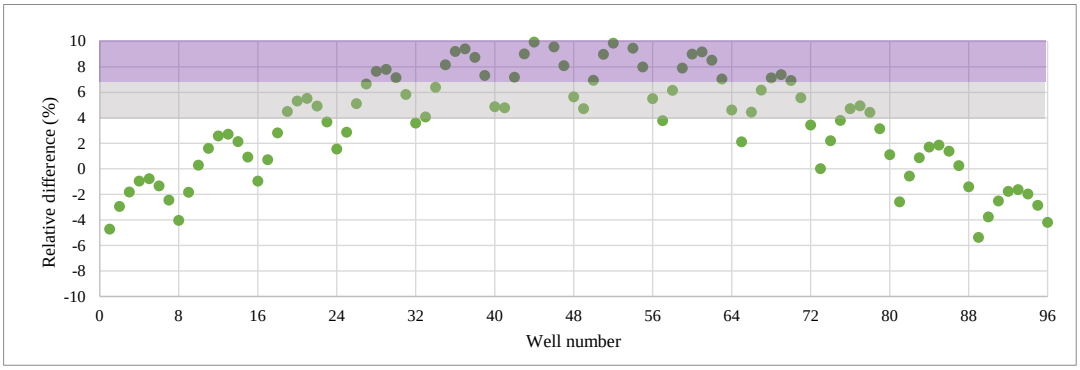

Figure 6.1 - Relative difference (%) between the reference dose of 2 Gy and the calculated planned dose for the wells of interest using (a) an 8x8 cm^2 field size, (b) a 30x30 cm^2 field size, and (c) a FFF beam. Coloured regions represent regions of greater dose homogeneity. Wells within these regions are the wells of interest. For the FFF configuration, the region of interest was delineated through two groups of wells whose planned dose presented a maximum difference of 3% between each group (grey-filled area = group 1; purple-filled area = group 2).

B. Influence of incubation time after irradiation

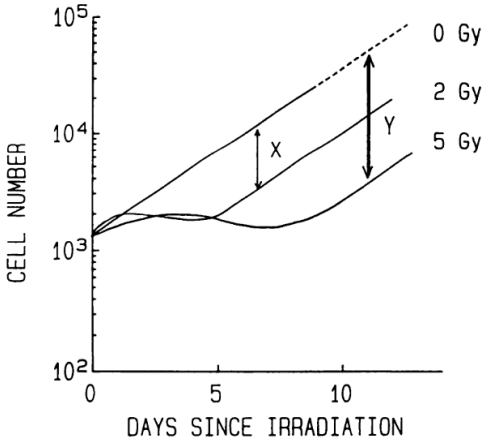

Figure 6.2 - Extrapolation of MTT growth curves for a specific cell line. For short incubation times, cell viability losses between irradiated and non-irradiated cells are underestimated. Also, growth of irradiated cells becomes exponential on day 5 at low doses, but later for higher doses. X = curve displacement for treatment with 2 Gy; Y = curve displacement for treatment with 5 Gy. Figure extracted from Price *et al.* (1990) [57].

C. Statistical analysis

This section presents the results of the statistical analysis performed on the results obtained throughout the work. Along with the statistical test applied, the corresponding figure of the results is indicated.

Table 6.1 – Multiple unpaired t tests of impact of transport on cell viability, 24 h (Figure 3.2, a).

	t ratio	df	Adjusted P Value
1×10^4	2.978	21.00	0.020421
2×10^4	1.462	22.00	0.158015
4×10^4	2.983	22.00	0.020421

Table 6.2 – Multiple unpaired t tests of impact of transport on cell viability, 48 h (Figure 3.2, b).

	t ratio	df	Adjusted P Value
1×10^4	2.262	21.00	0.067727
2×10^4	0.8504	22.00	0.404244
4×10^4	3.609	20.00	0.005249

Table 6.3 - Multiple comparisons of two-way ANOVA of influence of cell concentration, 24 h (Figure 3.3, a).

Tukey's multiple comparisons test	Summary	Adjusted P Value
1×10^4		
Control vs. 2 Gy	ns	0.6777
Control vs. 8 Gy	ns	0.9921
2 Gy vs. 8 Gy	ns	0.6414
2×10^4		
Control vs. 2 Gy	ns	0.8197
Control vs. 8 Gy	ns	0.0935
2 Gy vs. 8 Gy	ns	0.3700
4×10^4		
Control vs. 2 Gy	ns	0.8941
Control vs. 8 Gy	**	0.0084
2 Gy vs. 8 Gy	ns	0.0511

Table 6.4 - Multiple comparisons of two-way ANOVA of influence of cell concentration, 24 h (Figure 3.3, b).

Tukey's multiple comparisons test	Summary	Adjusted P Value
1×10^4		
Control vs. 2 Gy	ns	0.8349
Control vs. 8 Gy	***	0.0001
2 Gy vs. 8 Gy	***	0.0007
2×10^4		
Control vs. 2 Gy	****	<0.0001
Control vs. 8 Gy	****	<0.0001
2 Gy vs. 8 Gy	ns	0.8009
4×10^4		
Control vs. 2 Gy	ns	0.8071
Control vs. 8 Gy	****	<0.0001
2 Gy vs. 8 Gy	****	<0.0001

Table 6.5 - Multiple comparisons of two-way ANOVA of influence of incubation time (Figure 3.4).

Tukey's multiple comparisons test	Summary	Adjusted P Value
24 h		
0 vs. 2	ns	0.9442
0 vs. 5	ns	0.9919
0 vs. 10	ns	0.4658
2 vs. 5	ns	0.9983
2 vs. 10	ns	0.2360
5 vs. 10	ns	0.4916
48 h		
0 vs. 2	**	0.0017
0 vs. 5	ns	0.1218
0 vs. 10	ns	0.0964
2 vs. 5	ns	0.4991
2 vs. 10	ns	0.6480
5 vs. 10	ns	0.9979
72 h		
0 vs. 2	**	0.0040
0 vs. 5	**	0.0011
0 vs. 10	****	<0.0001
2 vs. 5	ns	0.9824
2 vs. 10	ns	0.0919
5 vs. 10	ns	0.2004

Table 6.6 - Multiple comparisons of two-way ANOVA of HAOA-AuNPs cytotoxicity on BxPC-3 cell line (Figure 3.5, a)

Tukey's multiple comparisons test	Summary	Adjusted P Value
24 h:0 µM vs. 24 h:50 µM	****	<0.0001
24 h:0 µM vs. 24 h:200 µM	****	<0.0001
24 h:0 µM vs. 24 h:400 µM	****	<0.0001
24 h:50 µM vs. 24 h:200 µM	ns	0.0569
24 h:50 µM vs. 24 h:400 µM	****	<0.0001
24 h:50 µM vs. 48 h:50 µM	ns	0.6272
24 h:200 µM vs. 24 h:400 µM	****	<0.0001
24 h:200 µM vs. 48 h:200 µM	ns	0.0999
24 h:400 µM vs. 48 h:400 µM	****	<0.0001
48 h:0 µM vs. 48 h:50 µM	***	0.0001
48 h:0 µM vs. 48 h:200 µM	****	<0.0001
48 h:0 µM vs. 48 h:400 µM	****	<0.0001
48 h:50 µM vs. 48 h:200 µM	ns	0.4728
48 h:50 µM vs. 48 h:400 µM	**	0.0027
48 h:200 µM vs. 48 h:400 µM	ns	0.3895

Table 6.7 - Multiple comparisons of two-way ANOVA of BBN-AuNPs cytotoxicity on BxPC-3 cell line (Figure 3.5, b)

Tukey's multiple comparisons test	Summary	Adjusted P Value
24h:0 µM vs. 24h:50 µM	ns	0.0637
24h:0 µM vs. 24h:200 µM	**	0.0067
24h:0 µM vs. 24h:400 µM	****	<0.0001
24h:50 µM vs. 24h:200 µM	ns	0.9831
24h:50 µM vs. 24h:400 µM	****	<0.0001
24h:50 µM vs. 48h:50 µM	****	<0.0001
24h:200 µM vs. 24h:400 µM	****	<0.0001
24h:200 µM vs. 48h:200 µM	****	<0.0001
24h:400 µM vs. 48h:400 µM	****	<0.0001
48h:0 µM vs. 48h:50 µM	****	<0.0001
48h:0 µM vs. 48h:200 µM	****	<0.0001
48h:0 µM vs. 48h:400 µM	****	<0.0001
48h:50 µM vs. 48h:200 µM	ns	0.6140
48h:50 µM vs. 48h:400 µM	*	0.0192
48h:200 µM vs. 48h:400 µM	ns	0.6140

Table 6.8 - Multiple comparisons of two-way ANOVA of HAOA-AuNPs during RT, 48 h (Figure 3.6).

Tukey's multiple comparisons test	Summary	Adjusted P Value
0:RT vs. 0:RT + 50 µM HAOA-AuNPs	ns	0.0550
0:RT vs. 0:RT + 200 µM HAOA-AuNPs	ns	0.1653
0:RT vs. 0:RT + 400 µM HAOA-AuNPs	****	<0.0001
0:RT vs. 2:RT	ns	0.1207
0:RT vs. 2:RT + 50 µM HAOA-AuNPs	****	<0.0001
0:RT vs. 2:RT + 200 µM HAOA-AuNPs	****	<0.0001
0:RT vs. 2:RT + 400 µM HAOA-AuNPs	****	<0.0001
0:RT vs. 3,5:RT	ns	0.9368
0:RT vs. 3,5:RT + 50 µM HAOA-AuNPs	ns	0.5241
0:RT vs. 3,5:RT + 200 µM HAOA-AuNPs	****	<0.0001
0:RT vs. 3,5:RT + 400 µM HAOA-AuNPs	****	<0.0001
0:RT vs. 5:RT	**	0.0014
0:RT vs. 5:RT + 50 µM HAOA-AuNPs	*	0.0107
0:RT vs. 5:RT + 200 µM HAOA-AuNPs	****	<0.0001
0:RT vs. 5:RT + 400 µM HAOA-AuNPs	****	<0.0001
0:RT + 50 µM HAOA-AuNPs vs. 0:RT + 200 µM HAOA-AuNPs	ns	>0.9999
0:RT + 400 µM HAOA-AuNPs vs. 2:RT + 400 µM HAOA-AuNPs	ns	>0.9999
0:RT + 400 µM HAOA-AuNPs vs. 3,5:RT + 400 µM HAOA-AuNPs	ns	0.3283
0:RT + 400 µM HAOA-AuNPs vs. 5:RT + 400 µM HAOA-AuNPs	ns	>0.9999
2:RT vs. 2:RT + 50 µM HAOA-AuNPs	***	0.0008
2:RT vs. 2:RT + 200 µM HAOA-AuNPs	****	<0.0001
2:RT vs. 2:RT + 400 µM HAOA-AuNPs	****	<0.0001
3,5:RT vs. 3,5:RT + 50 µM HAOA-AuNPs	ns	0.9976
3,5:RT vs. 3,5:RT + 200 µM HAOA-AuNPs	***	0.0008
3,5:RT vs. 3,5:RT + 400 µM HAOA-AuNPs	****	<0.0001
5:RT vs. 5:RT + 50 µM HAOA-AuNPs	ns	>0.9999
5:RT vs. 5:RT + 200 µM HAOA-AuNPs	***	0.0002
5:RT vs. 5:RT + 400 µM HAOA-AuNPs	****	<0.0001

Table 6.9 - Multiple comparisons of two-way ANOVA of HAOA-AuNPs during RT, 72 h (Figure 3.7).

Tukey's multiple comparisons test	Summary	Adjusted P Value
0:RT vs. 0:RT + 50 µM HAOA-AuNPs	ns	0.2634
0:RT vs. 0:RT + 200 µM HAOA-AuNPs	****	<0.0001
0:RT vs. 0:RT + 400 µM HAOA-AuNPs	****	<0.0001
0:RT vs. 2:RT	****	<0.0001
0:RT vs. 2:RT + 50 µM HAOA-AuNPs	****	<0.0001
0:RT vs. 2:RT + 200 µM HAOA-AuNPs	****	<0.0001
0:RT vs. 2:RT + 400 µM HAOA-AuNPs	****	<0.0001
0:RT vs. 3,5:RT	****	<0.0001
0:RT vs. 3,5:RT + 50 µM HAOA-AuNPs	****	<0.0001
0:RT vs. 3,5:RT + 200 µM HAOA-AuNPs	****	<0.0001
0:RT vs. 3,5:RT + 400 µM HAOA-AuNPs	****	<0.0001
0:RT vs. 5:RT	****	<0.0001
0:RT vs. 5:RT + 50 µM HAOA-AuNPs	****	<0.0001
0:RT vs. 5:RT + 200 µM HAOA-AuNPs	****	<0.0001
0:RT vs. 5:RT + 400 µM HAOA-AuNPs	****	<0.0001
0:RT + 200 µM HAOA-AuNPs vs. 2:RT + 200 µM HAOA-AuNPs	***	0.0005
0:RT + 200 µM HAOA-AuNPs vs. 3,5:RT + 200 µM HAOA-AuNPs	****	<0.0001
0:RT + 200 µM HAOA-AuNPs vs. 5:RT + 200 µM HAOA-AuNPs	****	<0.0001
0:RT + 400 µM HAOA-AuNPs vs. 2:RT + 400 µM HAOA-AuNPs	ns	0.0877
0:RT + 400 µM HAOA-AuNPs vs. 3,5:RT + 400 µM HAOA-AuNPs	ns	0.2137
0:RT + 400 µM HAOA-AuNPs vs. 5:RT + 400 µM HAOA-AuNPs	**	0.0013
2:RT vs. 2:RT + 50 µM HAOA-AuNPs	ns	0.6003
2:RT vs. 2:RT + 200 µM HAOA-AuNPs	****	<0.0001
2:RT vs. 2:RT + 400 µM HAOA-AuNPs	****	<0.0001
3,5:RT vs. 3,5:RT + 50 µM HAOA-AuNPs	ns	0.9991
3,5:RT vs. 3,5:RT + 200 µM HAOA-AuNPs	****	<0.0001
3,5:RT vs. 3,5:RT + 400 µM HAOA-AuNPs	****	<0.0001
5:RT vs. 5:RT + 50 µM HAOA-AuNPs	ns	0.9923
5:RT vs. 5:RT + 200 µM HAOA-AuNPs	**	0.0038
5:RT vs. 5:RT + 400 µM HAOA-AuNPs	****	<0.0001

Table 6.10 - Multiple comparisons of two-way ANOVA of BBN-AuNPs during RT, 48 h (Figure 3.8, a).

Tukey's multiple comparisons test	Summary	Adjusted P Value
0:RT vs. 0:RT + 50 µM BBN-AuNPs	****	<0.0001
0:RT vs. 0:RT + 200 µM BBN-AuNPs	****	<0.0001
0:RT vs. 2:RT	ns	0.1114
0:RT vs. 2:RT + 50 µM BBN-AuNPs	****	<0.0001
0:RT vs. 2:RT + 200 µM BBN-AuNPs	****	<0.0001
0:RT vs. 3,5:RT	ns	0.8857
0:RT vs. 3,5:RT + 50 µM BBN-AuNPs	**	0.0027
0:RT vs. 3,5:RT + 200 µM BBN-AuNPs	****	<0.0001
0:RT vs. 5:RT	**	0.0018
0:RT vs. 5:RT + 50 µM BBN-AuNPs	****	<0.0001
0:RT vs. 5:RT + 200 µM BBN-AuNPs	****	<0.0001
0:RT + 50 µM BBN-AuNPs vs. 2:RT + 50 µM BBN-AuNPs	ns	0.9814
0:RT + 50 µM BBN-AuNPs vs. 3,5:RT + 50 µM BBN-AuNPs	ns	0.9719
0:RT + 50 µM BBN-AuNPs vs. 5:RT + 50 µM BBN-AuNPs	ns	0.9212
0:RT + 200 µM BBN-AuNPs vs. 2:RT + 200 µM BBN-AuNPs	ns	0.5839
0:RT + 200 µM BBN-AuNPs vs. 3,5:RT + 200 µM BBN-AuNPs	ns	0.9983
0:RT + 200 µM BBN-AuNPs vs. 5:RT + 200 µM BBN-AuNPs	ns	0.4103
2:RT vs. 2:RT + 50 µM BBN-AuNPs	****	<0.0001
2:RT vs. 2:RT + 200 µM BBN-AuNPs	****	<0.0001
3,5:RT vs. 3,5:RT + 50 µM BBN-AuNPs	ns	0.1031
3,5:RT vs. 3,5:RT + 200 µM BBN-AuNPs	****	<0.0001
5:RT vs. 5:RT + 50 µM BBN-AuNPs	***	0.0002
5:RT vs. 5:RT + 200 µM BBN-AuNPs	****	<0.0001

Table 6.11 - Multiple comparisons of two-way ANOVA of BBN-AuNPs during RT, 72 h (Figure 3.8, b).

Tukey's multiple comparisons test	Summary	Adjusted P Value
0:RT vs. 0:RT + 50 μM BBN-AuNPs	****	<0.0001
0:RT vs. 0:RT + 200 μM BBN-AuNPs	****	<0.0001
0:RT vs. 2:RT	****	<0.0001
0:RT vs. 2:RT + 50 μM BBN-AuNPs	****	<0.0001
0:RT vs. 2:RT + 200 μM BBN-AuNPs	****	<0.0001
0:RT vs. 3,5:RT	****	<0.0001
0:RT vs. 3,5:RT + 50 μM BBN-AuNPs	****	<0.0001
0:RT vs. 3,5:RT + 200 μM BBN-AuNPs	****	<0.0001
0:RT vs. 5:RT	****	<0.0001
0:RT vs. 5:RT + 50 μM BBN-AuNPs	****	<0.0001
0:RT vs. 5:RT + 200 μM BBN-AuNPs	****	<0.0001
0:RT + 50 μM BBN-AuNPs vs. 2:RT + 50 μM BBN-AuNPs	****	<0.0001
0:RT + 50 μM BBN-AuNPs vs. 3,5:RT + 50 μM BBN-AuNPs	****	<0.0001
0:RT + 50 μM BBN-AuNPs vs. 5:RT + 50 μM BBN-AuNPs	****	<0.0001
0:RT + 200 μM BBN-AuNPs vs. 2:RT + 200 μM BBN-AuNPs	ns	>0.9999
0:RT + 200 μM BBN-AuNPs vs. 3,5:RT + 200 μM BBN-AuNPs	ns	0.6094
0:RT + 200 μM BBN-AuNPs vs. 5:RT + 200 μM BBN-AuNPs	ns	0.3917
2:RT vs. 2:RT + 50 μM BBN-AuNPs	****	<0.0001
2:RT vs. 2:RT + 200 μM BBN-AuNPs	****	<0.0001
3,5:RT vs. 3,5:RT + 50 μM BBN-AuNPs	****	<0.0001
3,5:RT vs. 3,5:RT + 200 μM BBN-AuNPs	****	<0.0001
5:RT vs. 5:RT + 50 μM BBN-AuNPs	****	<0.0001
5:RT vs. 5:RT + 200 μM BBN-AuNPs	****	<0.0001

Table 6.12 - Multiple comparisons of two-way ANOVA of impact of field size during RT with AuNPs (Figure 3.9).

Tukey's multiple comparisons test	Summary	Adjusted P Value
0 μM:8x8 cm^2 vs. 0 μM:30x30 cm^2	****	<0.0001
0 μM:20x20 cm^2 vs. 0 μM:30x30 cm^2	****	<0.0001
50 μM:8x8 cm^2 vs. 50 μM:30x30 cm^2	****	<0.0001
50 μM:20x20 cm^2 vs. 50 μM:30x30 cm^2	****	<0.0001
100 μM:8x8 cm^2 vs. 100 μM:30x30 cm^2	ns	0.0690
100 μM:20x20 cm^2 vs. 100 μM:30x30 cm^2	***	0.0001
200 μM:8x8 cm^2 vs. 200 μM:20x20 cm^2	**	0.0054

Table 6.13 - Multiple comparisons of two-way ANOVA of impact of free-flattening filter beam during RT with AuNPs (Figure 3.10).

Šídák's multiple comparisons test	Summary	Adjusted P Value
Group 1		
Control vs. 200 μM HAOA-AuNPs	****	<0.0001
Control vs. RT	ns	0.9823
Control vs. RT + 200 μM HAOA-AuNPs	****	<0.0001
200 μM HAOA-AuNPs vs. RT	****	<0.0001
200 μM HAOA-AuNPs vs. RT + 200 μM HAOA-AuNPs	**	0.0014
RT vs. RT + 200 μM HAOA-AuNPs	****	<0.0001
Group 2		
Control vs. 200 μM HAOA-AuNPs	****	<0.0001
Control vs. RT	ns	0.0573
Control vs. RT + 200 μM HAOA-AuNPs	****	<0.0001
200 μM HAOA-AuNPs vs. RT	ns	0.3893
200 μM HAOA-AuNPs vs. RT + 200 μM HAOA-AuNPs	****	<0.0001
RT vs. RT + 200 μM HAOA-AuNPs	****	<0.0001